



Evaluation of uncertainties in measurements





Evaluation of uncertainties in measurements

© 2010 PREPARED

The European Commission is funding the Collaborative project 'PREPARED Enabling Change' (PREPARED) within the context of the Seventh Framework Programme 'Environment'. All rights reserved. No part of this book may be reproduced, stored in a database or retrieval system, or published, in any form or in any way, electronically, mechanically, by print, photoprint, microfilm or any other means without prior written permission from the publisher

COLOPHON

Title

Evaluation of uncertainties in measurements

Report number

2011-021

Deliverable number

D 3.1.6.

Author(s)

Jean-Luc Bertrand-Krajewski, Alvaro Silva Ribeiro and Maria do Ceu Almeida

Quality Assurance

By Siao Sun and Joep van den Broeke

Document history

| Version | Team member | Status | Date update | Comments |
|---------|-------------|--------|---------------|---------------------------|
| 0 | JLBK | Draft | 29 Mar. 2011 | First draft |
| 1 | JLBK | Final | 22 Aug. 2011 | Final revision |
| 2 | JLBK | Final | 26 Sept. 2011 | Minor editing corrections |

This report is:

PU = Public

Summary

Assessing uncertainties is done systematically in almost all hard sciences research fields, and in more and more numerous engineering domains. In the field of urban water systems, this is still not a systematic and common practice. Therefore, one of the aims of PREPARED is to promote, to contribute and to exemplify how to systematically evaluate uncertainties in urban water systems.

Assessing uncertainties is necessary:

- to better quantify and to improve the quality of measurements;
- to better contribute in modelling, by accounting for uncertainties in model structures, inputs, parameters and outputs;
- to better help in decision making.

This PREPARED deliverable includes:

- an introduction to the two internationally recognized standards for assessment of measurement uncertainties (GUM Law of Propagation of uncertainties and the Monte Carlo method);
- three examples of application, with various levels of complexity, showing in detail how to apply the above methods for uncertainty assessment. The examples deal with sewer systems, but they can be easily transposed to other components of urban water systems.
- references to additional documents.

CONTENTS

| | |
|--|----|
| 1. OBJECTIVES | 3 |
| 2. STANDARDS FOR ASSESSMENT OF UNCERTAINTIES IN MEASUREMENTS..... | 4 |
| 2.1 Introduction | 4 |
| 2.2 Terminology | 4 |
| 2.3 General comments on uncertainty analysis and bias | 6 |
| 2.4 International standards for assessing uncertainty in measurements | 6 |
| 2.4.1 GUM method | 7 |
| 2.4.2 Monte Carlo Method..... | 10 |
| 2.5 Application of GUM and MCM..... | 12 |
| 3. EXAMPLE 1: APPLICATION OF TYPE B AND MONTE CARLO METHODS FOR UA IN CASE OF DISCHARGE AND VOLUME MEASUREMENTS IN A CIRCULAR SEWER PIPE | 13 |
| 3.1 Introduction..... | 13 |
| 3.2 Discharge measurement | 13 |
| 3.2.1 Type B method..... | 13 |
| 3.2.2 Monte Carlo method | 14 |
| 3.2.3 Comparison | 16 |
| 3.3 Volume measurement..... | 17 |
| 3.3.1 Type B method..... | 18 |
| 3.3.2 Monte Carlo estimation..... | 20 |
| 3.3.2.1 Effect of discretisation | 20 |
| 3.3.2.2 Effect of discretisation and random errors | 21 |
| 3.4 Appendix to example 1 | 23 |
| 3.4.1 Estimation of standard uncertainties in R , h and U | 23 |
| 3.4.2 Uncertainty in R | 23 |
| 3.4.3 Uncertainty in h | 24 |
| 3.4.4 Uncertainty in U | 25 |
| 3.4.5 Matlab source code for MC calculations..... | 26 |
| 4. EXAMPLE 2: ESTIMATION OF TSS AND COD POLLUTANT LOADS FROM CONTINUOUS TURBIDITY MEASUREMENTS IN TWO URBAN SEWER SYSTEMS | 27 |
| 4.1 Introduction..... | 27 |
| 4.2 Calculation of discharge and concentrations of TSS and COD..... | 27 |
| 4.2.1 Event load calculation | 27 |
| 4.2.2 Determination of dry weather contribution during storm events | 28 |
| 4.3 Application to the Chassieu catchment with a separate sewer system | 30 |
| 4.4 Application to the Ecully catchment with a combined sewer system..... | 31 |
| 5. EXAMPLE 3: UNCERTAINTY EVALUATION OF MULTI-SENSOR FLOW MEASUREMENT IN A SEWER SYSTEM USING MONTE CARLO METHOD | 34 |
| 5.1 Introduction..... | 34 |
| 5.2 Methodology | 34 |
| 5.3 Evaluation of measurement uncertainty using MCM..... | 37 |
| 5.4 Sensitivity analysis..... | 39 |
| 5.5 Discussion and conclusions..... | 42 |
| 6. REFERENCES | 44 |

1. OBJECTIVES

Assessing uncertainties is done systematically in almost all hard sciences research fields, and in more and more numerous engineering domains. In the field of urban water systems, this is still not a systematic and common practice. Therefore, one of the aims of PREPARED is to promote, to contribute and to exemplify how to systematically evaluate uncertainties in urban water systems.

Assessing uncertainties is necessary:

- to better quantify and to improve the quality of measurements;
- to better contribute in modelling, by accounting for uncertainties in model structures, inputs, parameters and outputs;
- to better help in decision making.

The objectives of this deliverable are as follows:

- to introduce the two internationally recognized standards for assessment of measurement uncertainties;
- to provide examples of application.

Many documents already exist: this deliverable will not replicate them, but cites and refers to them as much as necessary.

2. STANDARDS FOR ASSESSMENT OF UNCERTAINTIES IN MEASUREMENTS

This chapter includes a short introduction, the necessary terminology, some general comments, and a brief presentation of the two main internationally accepted methodologies for uncertainty assessment (GUM and MCM).

2.1 INTRODUCTION

The *measurement process* is the act of assigning a value to some physical variable, by operating sensors and instruments in conjunction with data acquisition and reduction procedures. In an ideal measurement, the value assigned by the measurement would be the actual value of the physical variable intended to be measured. However, measurement process and environmental errors bring in uncertainty in the correctness of the value resulting from the measurement. To give some measure of confidence to the measured value, measurement errors must be identified, and their probable effect on the result estimated. *Uncertainty is simply an interval estimate of possible set of values for the error in the reported results of a measurement.* The process of systematically quantifying error estimates is known as uncertainty analysis.

Monitoring of urban water processes should be governed *by the ability of the measurements to achieve the specific objectives within the allowable uncertainties.* Thus, measurement uncertainty assessment should be a key part of the entire monitoring program: description of the measurements, determination of error sources, estimation of uncertainties, and documentation of the results. Uncertainty considerations need to be integrated in all phases of the monitoring process, including planning, design, the decision whether to measure or not with specific instruments, and the carrying out of the measurements. In essence, this means that uncertainty must be considered even at the *definition-of-objectives* stage; the objectives should include a specification of the allowable uncertainty.

Along with this philosophy, rigorous application or integration of uncertainty assessment methodology is an integral part of all monitoring phases. The most important benefits of standardised uncertainty analysis implementation are:

- identification of the dominant sources of error, their effects on the result, and estimation of the associated uncertainties,
- facilitation of meaningful and efficient communication of data quality,
- facilitation of selecting the most appropriate and cost effective measurement devices and procedures for a given measurement,
- consideration and reduction of the risks in decision making, and
- evidence of compliance with regulations.

2.2 TERMINOLOGY

Terminology in metrology is very specific and confusion with usual or ancient wordings should be avoided. Some key definitions are provided hereafter. More details are given in the dedicated international standards and especially in the VIM - International Vocabulary of Metrology (JCGM, 2008, 2010). Additional and more specific definitions are also given in ISO (2008a, 2008b, 2009a, 2009b).

- **Measurand**: quantity intended to be measured.
- **Uncertainty (VIM definition)**: non-negative parameter characterizing the dispersion of the quantity values being attributed to a measurand, based on the information used. This VIM definition remains very similar to the definition of the standard deviation. This is why the GUM (ISO, 2008a) provides a more specific definition, with three notes:
- **Uncertainty (GUM definition)**: parameter, associated with the result of a measurement, that characterizes the dispersion of the values that could reasonably be attributed to the measurand.
 - NOTE 1 The parameter may be, for example, a standard deviation (or a given multiple of it), or the half-width of an interval having a stated level of confidence.
 - NOTE 2 Uncertainty of measurement comprises, in general, many components. Some of these components may be evaluated from the statistical distribution of the results of series of measurements and can be characterized by experimental standard deviations. The other components, which also can be characterized by standard deviations, are evaluated from assumed probability distributions based on experience or other information.

- NOTE 3 It is understood that the result of the measurement is the best estimate of the value of the measurand, and that all components of uncertainty, including those arising from systematic effects, such as components associated with corrections and reference standards, contribute to the dispersion.
- **Measured quantity value:** measured value of a quantity measured value, quantity value representing a measurement result.
- **True value or true quantity value:** quantity value consistent with the definition of a quantity. A true value is usually unknown.
- **Measurement accuracy:** closeness of agreement between a measured quantity value and a true quantity value of a measurand. (See also Figure 2.1).
- **Measurement trueness:** closeness of agreement between the average of an infinite number of replicate measured quantity values and a reference quantity value. (See also Figure 2.1).
- **Measurement precision:** closeness of agreement between indications or measured quantity values obtained by replicate measurements on the same or similar objects under specified conditions.
- **Measurement error:** measured quantity value minus a reference quantity value.
- **Systematic measurement error:** component of measurement error that in replicate measurements remains constant or varies in a predictable manner.
- **Measurement bias:** estimate of a systematic measurement error.
- **Random measurement error:** component of measurement error that in replicate measurements varies in an unpredictable manner.
- **Repeatability condition of measurement:** condition of measurement, out of a set of conditions that includes the same measurement procedure, same operators, same measuring system, same operating conditions and same location, and replicate measurements on the same or similar objects over a short period of time.
- **Reproducibility condition of measurement:** condition of measurement, out of a set of conditions that includes different locations, operators, measuring systems, and replicate measurements on the same or similar objects.
- **Measurement reproducibility:** measurement precision under reproducibility conditions of measurement.
- **Standard measurement uncertainty:** measurement uncertainty expressed as a standard deviation.
- **Combined standard measurement uncertainty:** standard measurement uncertainty that is obtained using the individual standard measurement uncertainties associated with the input quantities in a measurement model.
- **Relative standard measurement uncertainty:** standard measurement uncertainty divided by the absolute value of the measured quantity value.
- **Expanded measurement uncertainty:** expanded uncertainty product of a combined standard measurement uncertainty and a factor larger than the number one.
- **Coverage interval:** interval containing the set of true quantity values of a measurand with a stated probability, based on the information available.
- **Coverage probability:** probability that the set of true quantity values of a measurand is contained within a specified coverage interval.
- **Coverage factor:** number larger than one by which a combined standard measurement uncertainty is multiplied to obtain an expanded measurement uncertainty.
- **Measurement function:** function of quantities, the value of which, when calculated using known quantity values for the input quantities in a measurement model, is a measured quantity value of the output quantity in the measurement model.
- **Influence quantity:** quantity that, in a direct measurement, does not affect the quantity that is actually measured, but affects the relation between the indication and the measurement result.
- **Correction:** compensation for an estimated systematic effect.

Figure 2.1 illustrate some of the above definitions.

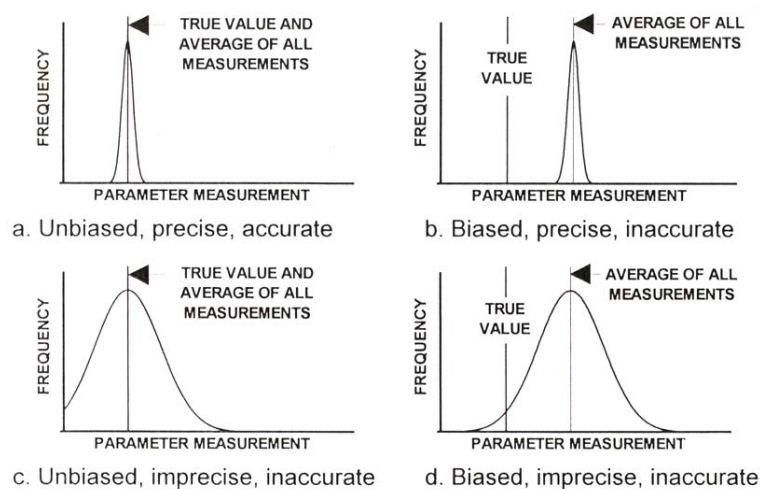


Figure 2.1: Illustration of measurement error concepts (AIAA, 1995)

2.3 GENERAL COMMENTS ON UNCERTAINTY ANALYSIS AND BIAS

The following paragraphs are adapted from Bertrand-Krajewski and Muste (2007).

Uncertainty analysis (UA) is a rigorous methodology for estimating uncertainties in measurements and in the results calculated from them. It combines statistical and engineering concepts. The analysis must be done in a manner that can be systematically applied to each step in the data uncertainty assessment determination.

Biases are usually very difficult to detect and remove. Sensor calibration with links to primary or secondary standards is a way to evaluate and remove (by correction) biases. However, sensor calibration qualifies the sensor itself, and not necessarily its use in a given location under given conditions which may themselves be the source of additional bias. This aspect should be accounted for as much as possible, as even relatively small biases may have dramatic effects on the final results from monitoring programmes (Fletcher and Deletic, 2007). If biases can be detected and assessed, they can be accounted for in the uncertainty assessment. In other cases, correct information on systematic errors is non-existent or very weak, and estimations are not possible. An alternative method in this case may be to simulate scenarios, i.e. to simulate the effects of possible systematic errors on the final results, in order to answer questions like “what if...” (e.g. how would the discharge and its uncertainty change if the water level sensor had a bias of + 2 cm?). In all cases, investigation to identify and remove possible biases, even if it is difficult, is a very important task to be carried out with the highest degree of rigour and intellectual honesty.

Frequently, instrumentation errors are the only ones dealt with in estimating uncertainties. This is unfortunate, because in many situations errors such as those induced by flow-sensor interaction, flow characteristics, and measurement operation are frequently larger than the instrument errors. This is why, as much as possible, the location and conditions of use of sensors should be accounted for to evaluate the total resulting uncertainty. For example, a water level sensor may have an instrument uncertainty (evaluated by means of an adequate calibration with certified standards) of ± 1 mm. If this sensor is used in a sewer system where the water is not still and perfectly horizontal, but moves downstream and generates small waves at the surface with possible secondary currents, leading to a non-horizontal free surface, the final uncertainty may reach ± 1 cm or more (see examples in Chapter 3). Conceptual biases (i.e. errors that might stand between concept and measurement) are generated during the test design and data analysis through idealisations (assumptions) in the data interpretation equations, use of equations which are incomplete and do not acknowledge all the significant factors, or by not measuring the correct variable (Moffat, 1988). Despite the potential importance of conceptual biases, and the challenging in assigning significance to what has been measured, this category of uncertainty is beyond the scope of this deliverable and will not be further discussed.

2.4 INTERNATIONAL STANDARDS FOR ASSESSING UNCERTAINTY IN MEASUREMENTS

The first internationally unified frame for UA in measurements was the GUM – Guide for Uncertainty in Measurements, published in 1993 (GUM, 1993), re-published with some revisions in 1995 and also as a

Evaluation of uncertainties in measurements – Report n° 2011-021

European standard in 1999 (ENV 13005, 1999). GUM is based on statistical methods. Since its publication, it has been revised, adapted and completed as parts of a new Guide for Uncertainty in Measurement (abbreviated as the *Guide*) elaborated at international level by the JCGM – Joint Committee for Guides in Metrology convened by the Bureau International des Poids et Mesures (BIPM), the International Electrotechnical Commission (IEC), the International Organization for Standardization (ISO), and the International Organization of Legal Metrology (OIML). The Supplement 1 published in 2008 introduces the Monte Carlo method for uncertainty assessment.

In this document, we will refer to the following parts of the *Guide*:

- As the global introduction for all concepts and methods:
ISO (2009a). *ISO/IEC Guide 98-1:2009(E) Uncertainty of measurement – Part 1: Introduction to the expression of the uncertainty in measurement*. Geneva (Switzerland): ISO, September 2009, 32 p.
- As Guide for uncertainty in measurements method (abbreviated as GUM in this deliverable):
ISO (2008a). *ISO/IEC Guide 98-3:2008(E) Uncertainty of measurement - Part 3: Guide to the expression of uncertainty in measurement (GUM: 1995)*. Geneva (Switzerland): ISO, December 2008, 130 p.
- As Monte Carlo method (abbreviated as MCM in this deliverable):
ISO (2008b). *ISO/IEC Guide 98-3/Suppl.1:2008(E) Uncertainty of measurement - Part 3: Guide to the expression of uncertainty in measurement (GUM: 1995) Supplement 1: Propagation of distributions using a Monte Carlo method*. Geneva (Switzerland): ISO, December 2008, 98 p.
ISO (2009b). *ISO/IEC Guide 98-3/S1/AC1:2009(E) Uncertainty of measurement - Part 3: Guide to the expression of uncertainty in measurement (GUM: 1995), Supplement 1: Propagation of distributions using a Monte Carlo method, Technical corrigendum 1*. Geneva (Switzerland): ISO, May 2009, 2 p.

GUM and MCM are also referred to as the “propagation of uncertainties” method and the “propagation of distributions” method, respectively.

This deliverable cannot reproduce the full content of the above detailed standards: a brief introduction is presented below, and examples are given in Chapters 3 to 5. It is the responsibility of the reader, when estimating uncertainties in measurements, to get an original version of the above standards and to apply the methods. For the PREPARED project, the authors of this deliverable may assist the user in case some difficulties occur in applying the methods.

The following sections are adapted from Muste *et al.* (2011).

2.4.1 GUM method

The GUM implementation entails the following steps:

Define the measurement process. A mathematical relationship of the measurement relates the measurand and input quantities. The measurement process has to provide an estimate (measurement) of each input quantity and the influence quantities involved in the measurement process.

Evaluate the standard uncertainty of each input estimate $u(x_i)$. Standard uncertainties can be evaluated using statistical methods (Type A) or other methods (Type B).

Type A evaluation. The standard uncertainty $u(x_i)$ of an input quantity X_i determined from n independent repeated observations is $u(x_i) = s(\bar{X}_i)$, calculated as follows:

$$s^2(\bar{X}_i) = \frac{s^2(x_{ik})}{n} \quad \text{eq. 1}$$

where

$$s^2(x_{ik}) = \frac{1}{n-1} \sum_{k=1}^n (x_{ik} - \bar{x}_i)^2 \quad \text{eq. 2}$$

$$\bar{x}_i = \frac{1}{n} \sum_{k=1}^n x_{ik} \quad \text{eq. 3}$$

The variable X_i is a random variable subjected to n independent observations (large number, i.e., more than 30), x_{ik} obtained under the same measurement conditions. Based on the available data, several situations can be distinguished [small measurement sample and knowledge from one set of previous observations, small measurement sample and knowledge from several sets of previous observations, and large measurement sample of current measurements (recommended)]. In Type A evaluations of measurement uncertainties, the assumption is often made that the distribution best describing the quantity is Gaussian. When uncertainties are determined from a small number of values, the corresponding distribution can be taken as a t -distribution.

Type B evaluation. Type B evaluations are those carried out by means other than the statistical analysis of a series of observations. This evaluation type is necessary when no current measurements or one (single) measurement are available. Consequently, previous knowledge is required. As Type B assessments have to ensure similar confidence levels as those obtained for Type A evaluations, they require a knowledge of the probability distribution associated with the uncertainty and the associated degree of freedom.

Type B standard uncertainty is based on the expected dispersion of measurements and the assumed probability distribution. The dispersion a_i is the estimated semi-range of a component of uncertainty associated with an input estimate x_i , as defined in Figure 2.2. The probability distribution can take a variety of forms, but is generally acceptable to assign well-defined geometric shapes (i.e., rectangular, Gaussian, triangular, asymmetric) for which the standard uncertainty can be obtained from a single calculation (see Figure 2.2). Typical examples of rectangular probability distributions include (ISO, 2005): maximum instrument drift between calibrations; error due to limited resolution of an instrument's display or digitizer; and manufacturers' tolerance limits. A normal probability distribution can also be used in association with calibration certificates quoting a confidence level (or coverage factor) with the expanded uncertainty. The triangular probability distribution is used when the only information available about a quantity is the maximum bounds within which all values of the quantity are assumed to lie. In some measurement situations, the upper and lower bounds for an input quantity are not symmetrical with respect to the best estimate due to, for example, a drift in the instrument. For such situations, the asymmetric distribution would be appropriate for estimating the standard uncertainty.

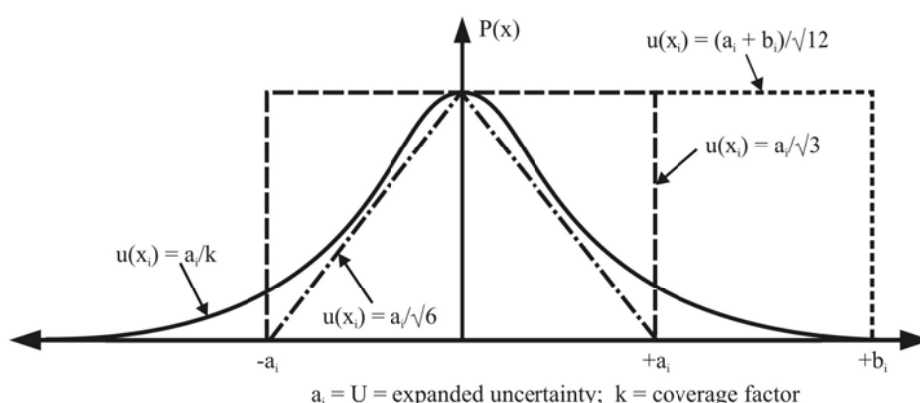


Figure 2.2: Probability distributions used to estimate Type B uncertainties (Muste *et al.*, 2011)

Add uncertainty components for each input variable. The various sources of uncertainties for a variable, irrespective of their provenance and type (A or B), are compounded using the root-sum-square (RSS) combination using:

$$u(x_i)^2 = \sum_{j=1}^K u(x_i)_j^2 \quad \text{eq. 4}$$

where $u(x_i)_j$ is the j -th standard uncertainty associated with the variable x_i .

Determine the estimated results. Use the measurement function f to calculate the measurand y in conjunction with the N determined input quantities x_i :

$$y = f(x_1, x_2, \dots, x_N) \quad \text{eq. 5}$$

Determine the combined standard uncertainty $u_c(y)$. The combined standard uncertainty is obtained using the following equation, frequently referred to as the LPU - Law of Propagation of Uncertainties:

$$u_c^2(y) = \sum_{i=1}^N \left(\frac{\partial f}{\partial x_i} \right)^2 u^2(x_i) + 2 \sum_{i=1}^{N-1} \sum_{j=i+1}^N \frac{\partial f}{\partial x_i} \frac{\partial f}{\partial x_j} u(x_i, x_j) \quad \text{eq. 6}$$

where f is the measurement function and each standard uncertainty $u(x_i)$ is estimated using either the Type A or B evaluation, or both. x_i and x_j are estimates of X_i and X_j , and $u(x_i, x_j) = u(x_j, x_i)$ is the estimated covariance associated with x_i and x_j :

$$u(x_i, x_j) = r(x_i, x_j) u(x_i) u(x_j) \quad \text{eq. 7}$$

where $r(x_i, x_j)$ is the correlation coefficient of x_i and x_j .

N is the number of input variables.

The partial derivatives, as called sensitivity coefficients c_i , are evaluated at $X_i = x_i$ using:

$$c_i = \frac{\partial f}{\partial X_i} \quad \text{eq. 8}$$

In case f has a very complicated analytical expression, its derivative may be difficult to establish analytically. It can be replaced by a numerical second order approximation:

$$c_i \approx \frac{f(x_i + \varepsilon) - f(x_i - \varepsilon)}{2\varepsilon} \quad \text{eq. 9}$$

where ε is very small compared to x_i (typically, one can use $\varepsilon = x_i / 1000$).

Determine the expanded uncertainty, using

$$U = k u_c(y) \quad \text{eq. 10}$$

where k is the coverage factor.

Ideally, uncertainty estimates are based upon reliable Type B and Type A evaluations with a sufficient number of observations such that using a coverage factor of $k = 2$ will ensure a confidence level close to 95 %. If any of these assumptions is not valid, the effective degree of freedom v_{eff} needs to be estimated using the Welch-Satterthwaite formula

$$v_{eff} = \frac{u_c^4(y)}{\sum_{i=1}^N \frac{u_i^4(y)}{v_i}} \quad \text{eq. 11}$$

where

$$u_c^2(y) = \sum_{i=1}^N u_i^2(y) = \sum_{i=1}^N (c_i u(x_i))^2 \quad \text{eq. 12}$$

and c_i is the sensitivity coefficient.

In case only a few observations are available, the value of k should be larger than 2 to estimate a 95 % confidence level, by replacing k by the Student t value which depends on the degrees of freedom (see application in Example 1, paragraph 3.2.1).

Report the results together with the combined and expanded uncertainty. The result of a measurement is expressed as:

$$Y = y \pm U = y \pm k u_c(y) \quad \text{eq. 13}$$

which is interpreted as the best estimate of the value attributable to the measurand Y , with $y - U$ to $y + U$ an interval that may be expected to encompass a large fraction of the distribution of values that could reasonably be

attributed to Y (typically, 95 % for $k = 2$). The reports for uncertainty estimates should present an uncertainty budget containing information such as probability distribution type, standard uncertainty, sensitivity coefficient, degrees of freedom, etc.

The method is summarized in Figure 2.3.

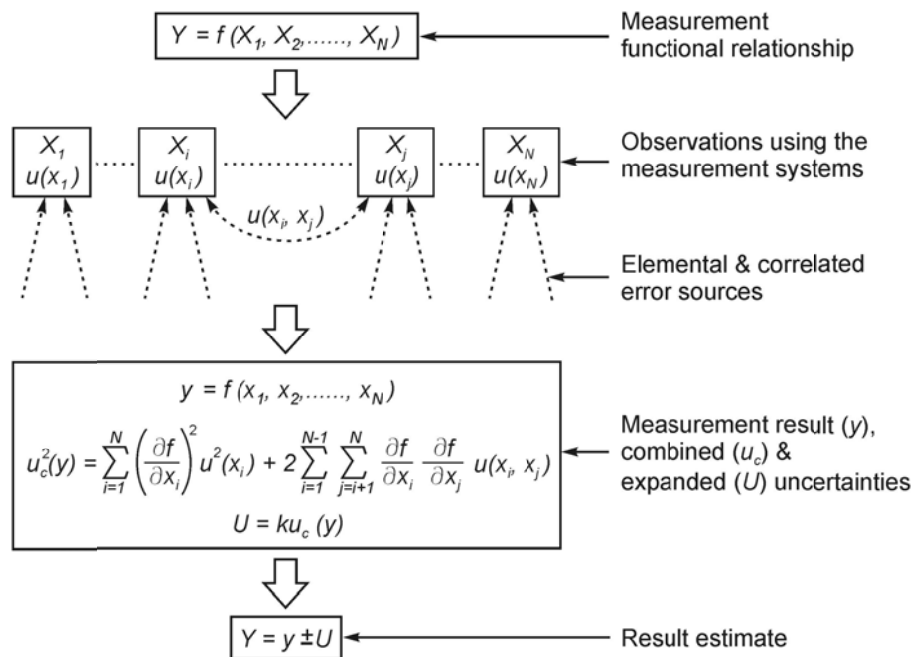


Figure 2.3: Flowchart illustrating the GUM implementation steps (Muste *et al.*, 2011)

2.4.2 Monte Carlo Method

The GUM uncertainty framework can be expected to work well in many circumstances. However, if there are assumptions that do not hold, the analysis might not give valid and meaningful results.

The main assumptions for a valid application of the above GUM methods are the following ones:

- the first order Taylor series (eq. 6.) is a valid approximation of $u_c(y)^2$, i.e. higher orders terms are negligible compared to first order ones and linearity is verified;
- all standard uncertainties $u(x_i)$ are small compared to x_i values;
- all uncertainties should be rather symmetrical around x_i values.

Evaluating the covariance terms in eq. 6 may be a difficulty in applying the GUM method. Indeed, if the same measured value is used to evaluate two or more quantities, then the correlation coefficient (eq. 7) of these two quantities is equal to one (e.g. the water level maybe used to estimate both flow cross section and wet perimeter in the Manning-Strickler equation). A more complex case is when standard uncertainties in measured values (and not measured values themselves) are correlated.

The Monte Carlo Method (MCM) is more frequently used, as the degree of difficulty is less (from a mathematical point of view) than GUM. As a rule of thumb, if GUM usage is proven to be favourable, it should be used as the adopted uncertainty framework, as it is faster once eq. 6 is established for a given measurement process. If not, MCM can be considered instead. The steps for implementing MCM are given below, most often conducted using software since manual calculation of large distributions is not feasible.

In case of doubt, it is recommended to compare GUM and MCM for a few cases and, according to the obtained results, to decide which method should be applied routinely.

The main principle of MCM consists to estimate M times the measurand Y by means of artificial (computer generated) samples of size M for each input quantity X_i . Each sample is generated with the appropriate probability distribution function - PDF (Gaussian, uniform, empirical, etc.) for each input quantity X_i . This is simple when all X_i -s are not correlated (no covariance) or when they are fully correlated (i.e. $r(X_i, X_j) = 1$). If samples should be partly correlated, specific techniques are necessary: if all PDFs are Gaussian, the *Guide* gives

all necessary information. If PDFs are not Gaussian, the problem may be more complex and specific statistical methods shall be applied, which can be found in the scientific literature (e.g. Gentle, 2004). Once the M values of the measurand are calculated, one calculates then the mean value \bar{y} and its empirical coverage interval $[y_{\text{low}}, y_{\text{high}}]$ determined from the percentiles of the PDF of the calculated measurand. One uses typically a 95% coverage interval.

The implementation steps of MCM are:

Select the number of trials M to be made (a value of $M = 10^6$ can often be expected to deliver approximately 95 % coverage interval for the output quantity, such that this length is correct to one or two significant decimal digits). As there is no guarantee that $M = 10^6$ or any specific pre-assigned number will suffice, an adaptive MCM (which selects M adaptively as the trials progress until various results of interest have stabilized in a statistical sense) is described in the *Guide*.

Sampling from probability distributions and evaluation of the model

N vectors with values x_{ij} of size M ($j = 1:M$) are drawn from the PDFs $g_{x_i}(\xi_i)$ for the N input quantities X_i . The N vectors maybe independent, partly or fully correlated depending on the appropriate assumptions. The measurand is then evaluated for each of the M draws from the PDFs for the N input quantities by using the measurement function (eq. 5). Draws are as x_1, \dots, x_N where the j -th draw x_j contains x_{1j}, \dots, x_{Nj} , and x_{ij} being a draw from the PDF for X_i . The measurand estimates y_j are:

$$y_j = f(x_{1j}, x_{2j}, \dots, x_{Nj}) \text{ for } j=1:M \tag{eq. 14}$$

Figure 2.4 graphically depicts both MCM and GUM methods for $N = 3$ independent input quantities X_i . On the left graph, the $g_{x_i}(\xi_i)$ $i= 1, 2, 3$, are Gaussian, triangular, and Gaussian, respectively, and the output PDF $g_Y(\eta)$ is asymmetric. The asymmetric distribution can be associated with non-linear models or asymmetric $g_{x_i}(\xi_i)$.

Sort model values into strictly increasing order, using the sorted model values to provide G , a discrete representation of the distribution function $G_Y(\eta)$ for the output quantity Y .

Estimate the mean of the output quantity y of Y . In addition, the associated standard uncertainty $u(y)$ can be estimated as equal to the estimated standard deviation $s(y)$ by using appropriate statistical methods.

Estimate an appropriate coverage interval for Y , for a stipulated coverage probability p , by applying the adaptive Monte Carlo procedure if necessary to provide (approximations to) the endpoints y_{low} and y_{high} of the required (probabilistically symmetric or shortest) $100 p$ % coverage interval for the output quantity. A numerical result is deemed to be stabilized if twice the standard deviation associated with it is less than the targeted numerical tolerance, associated with the standard uncertainty $u(y)$ as described.

The conditions for MCM application are (ISO, 2008, Chapter 5.10.1):

- f is continuous with respect to all X_i -s in the neighbourhood of the best estimates x_i of the X_i .
- the PDF for Y is:
 - continuous over the interval for which this PDF is strictly positive,
 - unimodal (single-peaked), and
 - strictly increasing (or zero) to the left of the mode and strictly decreasing (or zero) to the right of the mode.
- A sufficiently large value for M is used.

The MC method is summarised in Figure 2.4.

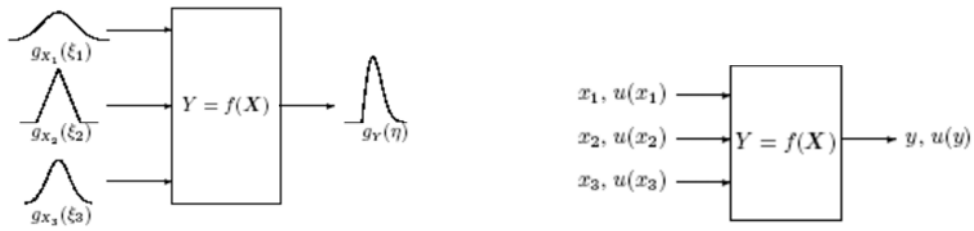


Figure 2.4: Simplified schematic diagram (ISO, 2008).

Left: propagation of distributions (MCM); right: law of propagation of uncertainties (GUM)

2.5 APPLICATION OF GUM AND MCM

In chapters 3 to 5, a few examples are provided to illustrate how to apply the GUM and MCM approaches of uncertainty assessment in measurements. For clarity, they may provide a few redundancies in explanations. The examples are dealing with discharge measurements, volume measurement and pollutant concentrations in collection systems. But they can easily be applied also in water supply, wastewater treatment, etc.

Additional information can be found in many papers e.g. Gruber *et al.*, 2005, Schilperoort *et al.*, 2009, Lacour, 2009.

Note: examples and references applying GUM or MCM to other urban water systems than sewer systems are particularly welcome, especially if they provide new information in compatibility with GUM and MCM. They will be included in future versions of the documents.

3. EXAMPLE 1: APPLICATION OF TYPE B AND MONTE CARLO METHODS FOR UA IN CASE OF DISCHARGE AND VOLUME MEASUREMENTS IN A CIRCULAR SEWER PIPE

3.1 INTRODUCTION

In this example, the uncertainty in the discharge and volume measured in a circular sewer pipe is calculated by means of two methods: i) the GUM type B method by application of the law of propagation of uncertainties LPU (ISO, 2009a) and ii) the Monte Carlo method (ISO, 2008, 2009b). For pedagogical reasons, most algebra and calculations are presented in detail. This example is copied, with minor modifications, from Bertrand-Krajewski (2011).

3.2 DISCHARGE MEASUREMENT

Let consider a circular concrete sewer pipe with radius $R = 0.5$. It is assumed i) that the pipe is circular and not affected by any deformation, and ii) that there are no deposits on the invert.

The discharge Q (m³/s) is then given by

$$Q(R, h, U) = S(h)U = R^2 \left[\text{Arccos} \left(1 - \frac{h}{R} \right) - \left(1 - \frac{h}{R} \right) \sqrt{1 - \left(1 - \frac{h}{R} \right)^2} \right] U \quad \text{eq. 15}$$

where h (m) is the water level and U (m/s) the mean flow velocity.

Calculations have been made with the following values:

$$R = 0.5 \text{ m}, u(R) = 0.001 \text{ m}$$

$$h = 0.7 \text{ m}, u(h) = 0.005 \text{ m}$$

$$U = 0.8 \text{ m/s}, u(U) = 0.05 \text{ m/s}.$$

Paragraph 3.4.1 explains how the standard uncertainties $u(R)$, $u(h)$ and $u(U)$ have been estimated.

The resulting discharge $Q = 0.4697$ m³/s. Note here that all results in the paper will be given with 4 or more digits only for illustration and comparison purposes. Under real conditions of application, one, two or three digits would be sufficient: the additional ones appear in *italic characters* in numerical values. However, it is of course recommended to keep the maximum number of digits in all intermediate calculations.

3.2.1 Type B method

All measured variables R , h and U are measured independently with different instruments and are not correlated. The effective degrees of freedom for the measurand are obtained using eq. 11, using the corresponding degrees of freedom for each variable (i.e. $\nu_R = 3$, $\nu_h = 59$, and $\nu_U = \infty$). The resulting effective degree of freedom for the measurand is 70256, a large value that for practical purposes can be considered an infinite value. Consequently, the law of propagation of uncertainty (LPU) can be written

$$u(Q)^2 = u(R)^2 \left(\frac{\partial Q}{\partial R} \right)^2 + u(h)^2 \left(\frac{\partial Q}{\partial h} \right)^2 + u(U)^2 \left(\frac{\partial Q}{\partial U} \right)^2 \quad \text{eq. 16}$$

The partial derivatives and their numerical values are equal to

$$\left(\frac{\partial Q}{\partial R} \right) = 2UR \text{Arccos} \left(1 - \frac{h}{R} \right) - 2U \sqrt{2hR - h^2} = 0.852 \text{ 638 427 096 m}^2/\text{s} \quad \text{eq. 17}$$

$$\left(\frac{\partial Q}{\partial h} \right) = 2U \sqrt{2hR - h^2} = 0.733 \text{ 212 111 192 m}^2/\text{s} \quad \text{eq. 18}$$

$$\left(\frac{\partial Q}{\partial U}\right) = R^2 \operatorname{Arccos}\left(1 - \frac{h}{R}\right) - (R-h)\sqrt{2hR-h^2} = 0.587\,229\,807\,114 \text{ m}^2 \quad \text{eq. 19}$$

In case algebra is considered too difficult, the above exact analytical expressions can be replaced by numerical estimations of partial derivatives by applying a second order approximation operator (several digits are given only for comparison between exact and approximated values):

$$\left(\frac{\partial Q}{\partial R}\right) = \frac{Q(R+\delta_R, h, U) - Q(R-\delta_R, h, U)}{2\delta_R} \approx \frac{0.469792 - 0.469775}{2 \cdot 10^{-5}} \approx 0.852\,638\,427\,287 \text{ m}^2/\text{s} \quad \text{eq. 20}$$

with $\delta_R = 10^{-5} \text{ m}$

$$\left(\frac{\partial Q}{\partial h}\right) = \frac{Q(R, h+\delta_h, U) - Q(R, h-\delta_h, U)}{2\delta_h} \approx \frac{0.469791 - 0.469776}{2 \cdot 10^{-5}} \approx 0.733\,212\,111\,117 \text{ m}^2/\text{s} \quad \text{eq. 21}$$

with $\delta_h = 10^{-5} \text{ m}$

$$\left(\frac{\partial Q}{\partial U}\right) = \frac{Q(R, h, U+\delta_U) - Q(R, h, U-\delta_U)}{2\delta_U} \approx \frac{0.469789 - 0.469777}{2 \cdot 10^{-5}} \approx 0.587\,229\,807\,111 \text{ m}^2 \quad \text{eq. 22}$$

with $\delta_U = 10^{-5} \text{ m/s}$

It is important to note that δ_x values should be chosen in such a way that $\delta_x \ll u(x)$.

Eq. 2 gives

$$u(Q)^2 = 7.2699 \cdot 10^{-7} + 1.3440 \cdot 10^{-5} + 8.6209 \cdot 10^{-4} = 8.7626 \cdot 10^{-4} \text{ m}^6/\text{s}^2 \quad \text{eq. 23}$$

and then the standard uncertainty $u(Q) = 0.0296 \text{ m}^3/\text{s} \approx 0.03 \text{ m}^3/\text{s}$.

With the enlargement factor $k_e = 2$, $Q \pm k_e \cdot u(Q) = 0.4697 \pm 0.0592 \text{ m}^3/\text{s}$.

i.e. a relative enlarged uncertainty $\frac{k_e u(Q)}{Q} = \frac{0.0593}{0.4697} = 0.126 = 12.6 \%$.

This can be interpreted as the true value Q has an approximately 95 % probability to lie in the interval $[Q - k_e u(Q), Q + k_e u(Q)] = [0.4106, 0.5289] \approx [0.41, 0.53]$.

Under real conditions, one would use $Q = 0.47 \pm 0.06 \text{ m}^3/\text{s}$.

One should note that, in eq. 23, the first term ($7.26 \cdot 10^{-7}$) is negligible compared to the two other ones: the contribution of the uncertainty in R to the total uncertainty in Q can be ignored. In addition, the contribution of the uncertainty in h is lower than the contribution of the uncertainty in U . However, this conclusion is not valid for all possible values of R , h and U : a specific analysis can be made for each particular set of values (R , h , U).

3.2.2 Monte Carlo method

For this example, $N = 10^6$ simulations are run. Details of calculation are given in Appendix 3.4.5.

The following samples are created:

N values of R normally distributed with mean value $\bar{R} = 0.5 \text{ m}$ and standard deviation $s(R) = 0.001 \text{ m}$.

N values of h normally distributed with mean value $\bar{h} = 0.7 \text{ m}$ and standard deviation $s(h) = 0.005 \text{ m}$.

N values of U normally distributed with mean value $\bar{U} = 0.8 \text{ m/s}$ and standard deviation $s(U) = 0.05 \text{ m/s}$.

All samples are independent and not correlated. The histogram of the water level sample is shown in Figure 3.1. The coefficients of correlation between the three samples are given in Table 3.1: the samples are clearly not correlated.

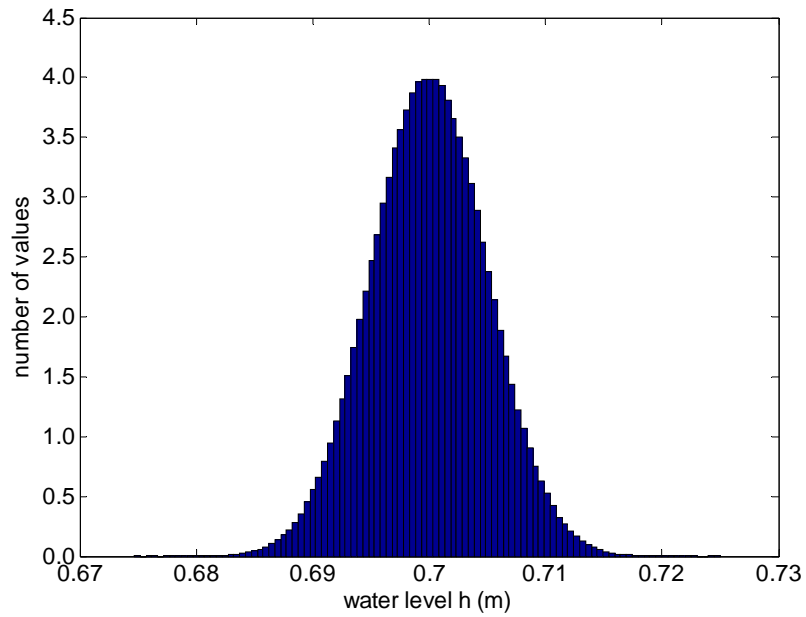


Figure 3.1: Histogram of the water level sample (one million values of h)

Table 3.1: Coefficients of correlation between the samples of the three variables R (m), h (m) and U (m/s)

| | R | h | U |
|-----|-----|---------|---------|
| R | 1 | -0.0004 | -0.0009 |
| h | | 1 | +0.0005 |
| U | | | 1 |

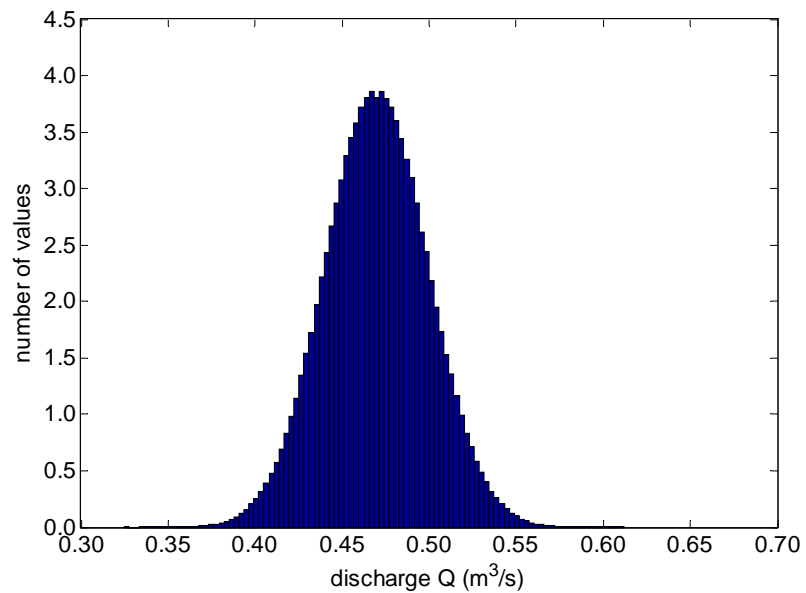


Figure 3.2: Histogram of the discharge sample (one million values of Q)

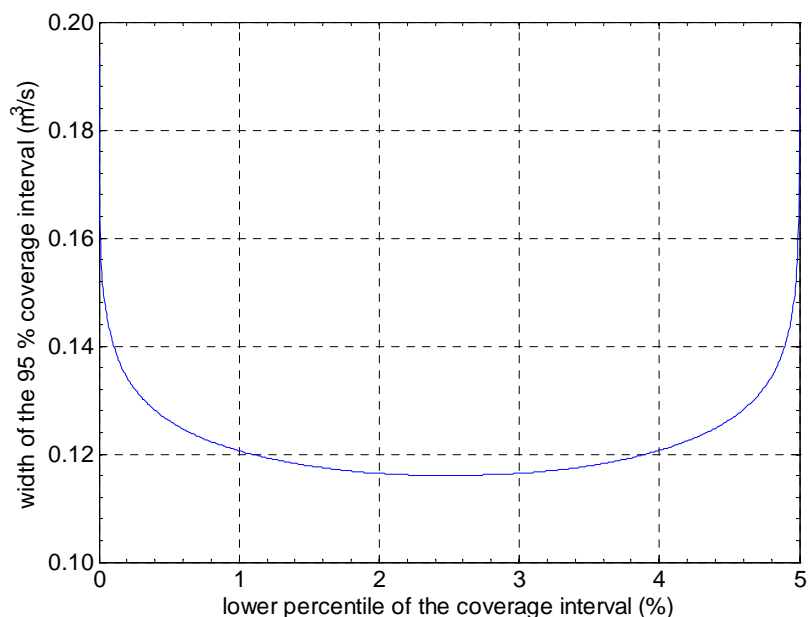


Figure 3.3: Width of the 95% coverage interval vs. the lower percentile of the coverage interval

The histogram of the resulting N values of discharge Q is shown in Figure 3.2. The mean value \bar{Q} is equal to $0.4698 \text{ m}^3/\text{s}$.

The variation of the width of the 95% coverage interval is represented in Figure 3.3. The shortest 95% coverage interval is $[0.4119, 0.5279] \approx [0.41, 0.53]$. In this simple case, the shortest 95 % coverage interval is equivalent to the traditional symmetrical 95 % confidence interval, but it may be different in other cases.

Simulations with other samples of the same size $N = 10^6$ give slightly different values. This is illustrated in Table 3.2 with 10 uncertainty evaluations. The standard deviation in the bottom line reveals that the dispersion of the results is very small and, in this case, negligible.

Table 3.2: Ten Monte Carlo uncertainty assessments (UA) with $N = 10^6$

| UA # | \bar{Q} (m ³ /s) | shortest 95 % CI | |
|--------------------|-------------------------------|------------------|--------|
| 1 | 0.4698 | 0.4115 | 0.5275 |
| 2 | 0.4698 | 0.4112 | 0.5273 |
| 3 | 0.4698 | 0.4118 | 0.5277 |
| 4 | 0.4698 | 0.4122 | 0.5283 |
| 5 | 0.4698 | 0.4118 | 0.5279 |
| 6 | 0.4698 | 0.4116 | 0.5275 |
| 7 | 0.4698 | 0.4118 | 0.5278 |
| 8 | 0.4698 | 0.4120 | 0.5278 |
| 9 | 0.4697 | 0.4114 | 0.5276 |
| 10 | 0.4698 | 0.4125 | 0.5284 |
| Mean value | 0.4698 | 0.4118 | 0.5278 |
| Standard deviation | 0.0000 | 0.0004 | 0.0003 |

3.2.3 Comparison

The type B method gives $\bar{Q} = 0.4698 \text{ m}^3/\text{s}$ and the 95 % confidence interval is $[0.4106, 0.5289]$ with $k_e = 2$.

The Monte Carlo method gives $\bar{Q} = 0.4698 \text{ m}^3/\text{s}$ and the shortest 95 % coverage interval is $[0.4119, 0.5279]$.

When considering only 2 digits as normally applied in practice, both results are considered similar.

If $k_e = 1.96$ is used instead of $k_e = 2$ (resp. a 95 % confidence interval instead of a 95.5 % confidence interval in case of a normal distribution), the type B interval becomes [0.4117, 0.5278] which is closer to the Monte Carlo shortest 95 % coverage interval.

Considering the Monte Carlo method as the reference method, one may conclude that, in this case, the type B method is validated and can be applied routinely, e.g. to discharge time series. The type B method requires preliminary algebra compared to the Monte Carlo method but, if it is validated, it runs faster than the Monte Carlo method when applied for example to time series. However, for single uncertainty assessment, the Monte Carlo method may be faster.

3.3 VOLUME MEASUREMENT

The second example deals with the estimation of the uncertainty in the volume calculated from discharge measurements. Let consider the volume $V(T)$ corresponding to the volume cumulated at time T over a duration θ ¹: $V(T)$ is the integral of the discharge $Q(t)$ from time $T-\theta$ to time T :

$$V(T) = \int_{t=T-\theta}^{t=T} Q(t) dt \quad \text{eq. 24}$$

In practice, $Q(t)$ is not measured continuously but with a discrete time step Δt . In addition, the true values of $Q(t)$ are not known: they are estimated by the discrete measured values $q(j\Delta t)$. The true volume $V(T)$ is then estimated approximately by the discrete sum $V_e(T)$:

$$V_e(T) = \sum_{j=1}^n q(T - (n - (j - 1))\Delta t)\Delta t \quad \text{eq. 25}$$

with n the number of time steps Δt for the duration $\theta = n\Delta t$ and j the time index.

Assuming that the uncertainty in the value of Δt is negligible, two main sources of uncertainty affect the estimate $V_e(T)$: i) uncertainties in the measured values $q(j\Delta t)$, which are estimated e.g. as shown in section 3.2 above, ii) uncertainties due to the discretisation of the true continuous signal $Q(t)$, which will be analysed hereafter. Uncertainties due to the discretisation have themselves two sources: i) the fact that the starting time of the measurement duration θ is arbitrarily, i.e. randomly, decided among all possible starting times uniformly distributed within the first time step Δt , ii) the fact that the exact integral of the continuous signal is replaced by a numerical sum of a limited number of discrete values.

Let re-write the discrete times as follows:

$$t_j = T - t_0 - (n - j + 1) \Delta t \quad \text{eq. 26}$$

t_0 is the time of the first discrete measurement of the discharge. It is considered as a random variable within the first time step window $[T - n\Delta t, T - (n - 1)\Delta t]$. Once t_0 is chosen, all subsequent discrete times t_j are determined by eq. 26.

The measured discharge $q(t_j)$ can be written:

$$q(t_j) = Q(t_j) + e(t_j) \quad \text{eq. 27}$$

with $Q(t_j)$ the true value of the discharge Q and e the error (i.e. the difference between the true but unknown value Q and the measured value q) at time t_j . The variance of $q(t_j)$ is equal to the variance of $e(t_j)$ as $Q(t_j)$ is the true value. Consequently,

$$u(q(t_j))^2 = u(e(t_j))^2 = \text{var}(e(t_j)) \quad \text{eq. 28}$$

¹ If the duration θ start at $t = 0$, then $V(T)$ is the integral from $t = 0$ to $T = \theta$. As, in many cases, θ may not necessarily coincide with 0 (zero), especially in case of e.g. successive storm events, we have adopted the more generic (but a little more complex notation) from $T-\theta$ to T .

eq. 27 and the algebra presented in section 3.3.1 hereafter are a simplified re-writing of a more detailed approach presented in Joannis and Bertrand-Krajewski (2009).

In order to illustrate the application of the above concepts and equations, true values of $Q(t)$ and $V(T)$ are necessary. That is the reason why a fictitious reference hydrograph $Q(t)$ has been created as the true value of a discharge time series (Figure 3.4). It corresponds to a 24 hour hydrograph at the outlet of a combined sewer system from 00:00 to 23:59 (1440 minutes) with a storm event occurring during the night between 04:00 and 06:00 (minutes 240 to 360). The hydrograph is the sum of constant and sinus continuous functions, allowing calculating the exact true value of the volume $V(T)$ in 24 hours, equal to 3000 m³. The uncertainty in estimates $V_e(T)$ will be evaluated by both the type B approach and Monte Carlo simulations.

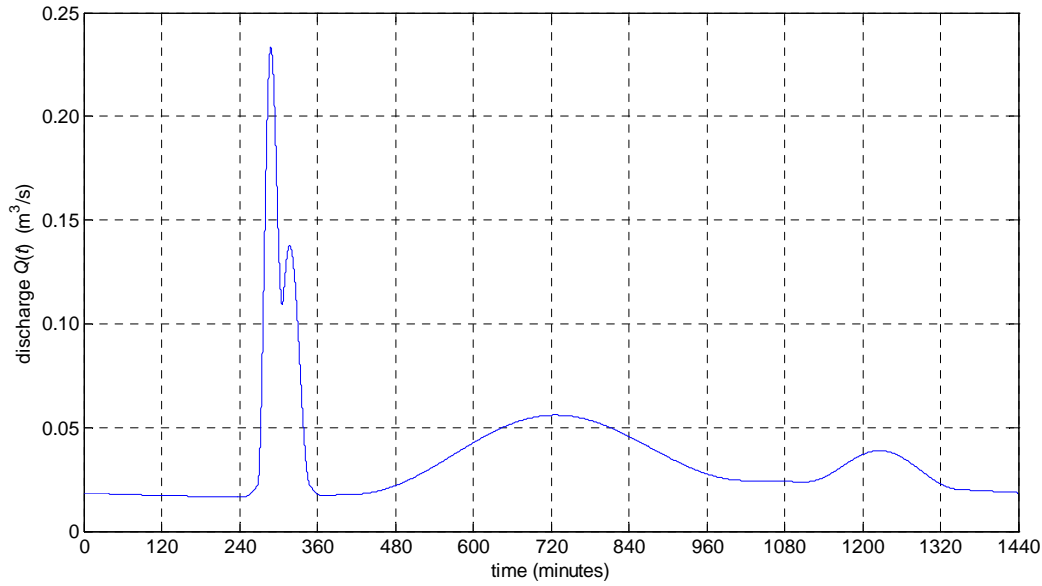


Figure 3.4: Fictitious 24 hour reference hydrograph

3.3.1 Type B method

Let define

$$\Delta Q(t_j) = \left(\frac{V(T)}{n\Delta t} \right) - Q(t_j) \quad \text{eq. 29}$$

$\Delta Q(t_j)$ is the distance between each true discharge value $Q(t_j)$ and the true mean discharge, in the interval $[T-\theta, T]$. Each discharge value is considered here as an approximation of the mean value: this allows distributing the error in the estimate $V_e(T)$ equally for each time t_j . This hypothesis, combined with eq. 26 and eq. 27, leads to

$$V_e(T) = V(T) + \sum_{j=1}^n [\Delta Q(t_j) + e(t_j)] \Delta t \quad \text{eq. 30}$$

With the hypothesis that Δt has a negligible uncertainty, it is convenient to re-write the above equation as follows:

$$\frac{V_e(T)}{\Delta t} = \frac{V(T)}{\Delta t} + \sum_{j=1}^n [\Delta Q(t_j) + e(t_j)] \quad \text{eq. 31}$$

Then, accounting for the fact that $V(T)$ is the true value of the volume and consequently has no uncertainty, the LPU applied by accounting for all covariances leads to

$$\begin{aligned} \frac{u(V_e(T))^2}{\Delta t^2} = & \sum_{j=1}^n u(e(t_j))^2 + \sum_{j=1}^n u(\Delta Q(t_j))^2 + 2 \sum_{j=1}^{n-1} \sum_{k=j+1}^n u(\Delta Q(t_j), \Delta Q(t_k)) \\ & + 2 \sum_{j=1}^{n-1} \sum_{k=j+1}^n u(e(t_j), e(t_k)) + 2 \sum_{j=1}^{n-1} \sum_{k=j+1}^n u(\Delta Q(t_j), e(t_k)) \end{aligned} \quad \text{eq. 32}$$

According to eq. 28, $u(e(t_j)) = u(q(t_j))$.

According to eq. 29, $u(\Delta Q(t_j)) = u(Q(t_j))$ and $u(\Delta Q(t_j), \Delta Q(t_k)) = u(Q(t_j), Q(t_k))$ as $V(T)$ is a true value. If t_j and t_k are known, $Q(t_j)$ and $Q(t_k)$ are also known and have no uncertainty. They can be considered as random variables only if t_j and t_k are random variables. If the time step Δt is fixed, the possible variations of the j -th measurement $q(t_j)$ used in eq. 25 correspond to uniformly distributed variations of t_j in the time step interval $[(T-n-j-1)\Delta t, (T-n-j)\Delta t]$. In practice, all values of t_j are fixed if t_0 is given (eq. 26). Consequently, the possible variations of $q(t_j)$ are only due the variations of t_0 , which is the key variable when considering uncertainties due to discretisation. $u(Q(t_j))^2$ and $u(Q(t_j), Q(t_k))$ are thus respectively the variance and covariance of the discharge values when t_0 is randomly chosen in a time interval of length equal to Δt . In practice, the continuous true discharge Q is not known: only discrete measured values q are available. A model is then necessary to interpolate between discrete values q to re-build a virtual continuous signal. It is important to note that the covariance $u(Q(t_j), Q(t_k))$ is not the covariance between successive values $Q(t_j)$, $Q(t_j + \Delta t)$, $Q(t_j + 2\Delta t)$, etc., but the covariance of the values of $Q(t_j)$ when t_j is varying *within* the j -th time step when t_0 is chosen randomly to start a measurement period.

Considering lastly that i) there is no covariance between ΔQ and e (measurement errors are not correlated with discretisation errors) and ii) there is no covariance between measurement errors (only random errors are considered, systematic errors have been corrected), eq. 32 can be simplified and re-written as follows:

$$u(V_e(T))^2 = \Delta t^2 \left(\underbrace{\sum_{j=1}^n u(q(t_j))^2}_{(A)} + \underbrace{\sum_{j=1}^n u(\Delta Q(t_j))^2}_{(B)} + 2 \underbrace{\sum_{j=1}^{n-1} \sum_{k=j+1}^n u(\Delta Q(t_j), \Delta Q(t_k))}_{(C)} \right) \quad \text{eq. 33}$$

To simulate a real measurement process, discrete hydrographs have been generated. An example is shown in Figure 3.5 with $\Delta t = 30$ min and random errors $e(t_j)$ sampled from normal distributions with mean values equal to zero and standard deviations equal to 7.5 % of the true values $Q(t_j)$, i.e. $u(q(t_j)) = 0.075 \times Q(t_j)$. Δt is large (30 min) only to facilitate the legibility of Figure 3.5. $V_e(T)$ is equal to 2967 m³.

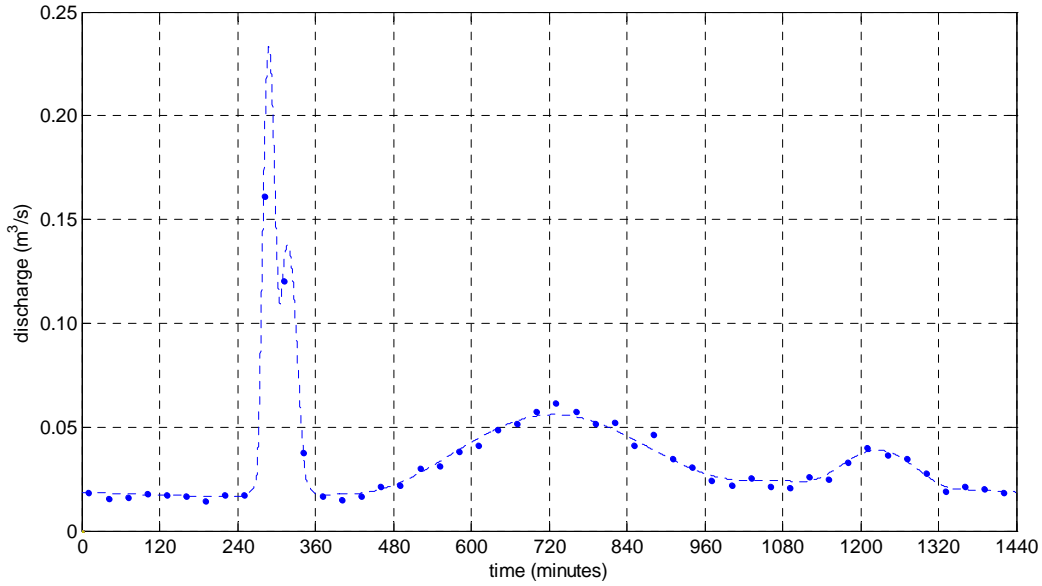


Figure 3.5: Example of discrete measurements with $\Delta t = 30$ min and relative standard uncertainties in q values equal to $0.075 \times q$. For comparison, the true signal is represented by the dashed line

eq. 33 contains 3 terms:

- A corresponds to the random errors in measurements: $A = 1541 \text{ m}^6$.
- B corresponds to the variances linked to the discretisation: $B = 15409 \text{ m}^6$.
- C corresponds to the covariances linked to the discretisation: $C = -7291 \text{ m}^6$.

The total uncertainty in $V_e(T)$ is then given by $u(V_e(T)) = \sqrt{A+B+C} = 98 \text{ m}^3$. With an enlargement factor $k_e = 2$, $V_e(T) \pm k_e u(V_e(T)) = 2967 \pm 196 \text{ m}^3$. The corresponding interval is [2771; 3163].

The contribution of the discretisation to the total uncertainty is equal to $(B+C)/(A+B+C) = 84 \%$ of the total uncertainty, while the contribution of random errors is only 16 %.

3.3.2 Monte Carlo estimation

Monte Carlo simulations have been run in order to illustrate a more detailed analysis of the uncertainty in $V_e(T)$. The first step will consider only discretisation. The second step will consider both discretisation and measurement uncertainties as sources of uncertainty in $V_e(T)$.

3.3.2.1 Effect of discretisation

This step aims to answer the following question: how discretisation of the true hydrograph $Q(t)$ with a time step Δt may affect the estimate $V_e(T)$? Measured values $q(t_j)$ are considered with no uncertainties.

Fourteen time steps ($s = 1:14$) have been analysed, respectively equal to 1, 2, 5, 10, 15, 20, 30, 45, 60, 90, 120, 180, 240 and 360 minutes. Long-time steps have been tested only for illustration purposes as such high values are not realistic for discharge measurements. For each value Δt_s , the starting time t_0 is randomly set within the first time step $[0, \Delta t_s]$. One million ($N = 10^6$) simulations of t_0 have been generated by

$$t_{0si} = \alpha_i \Delta t_s \quad \text{eq. 34}$$

with α_i a random number between 0 and 1 and i the Monte Carlo simulation index $i = 1:N$.

As a result, N values of $V_e(T)$ are calculated for each time step Δt_s :

$$V_e(T)_{si} = \left(\sum_{k=1}^{m_s} Q(t_{0si} + (k-1)\Delta t_s) \right) \Delta t_s \quad \text{eq. 35}$$

with m_s the number of measured discrete values for each time step Δt_s

$$m_s = \frac{1440}{\Delta t_s} \quad \text{eq. 36}$$

Results are given in Figure 3.6. On each box plot, the central horizontal line indicates the median value, the central box is delimited by the first (bottom) and third (top) quartiles, and the extremities of the dashed lines represent the minimum (bottom) and maximum (top) values. Mean values, standard deviations and shortest 95 % coverage intervals are given in Table 3.3. All mean values are equal to 3000 m³.

For all time steps from 1 to 20 minutes, the discretisation has a negligible effect: $V(T)$ is always precisely estimated by $V_e(T)$. For time steps ranging from 30 to 60 minutes, a significant dispersion of the values is observed. For example, for $\Delta t = 45$ min, the mean is equal to 3000 m³, the median is equal to 2976 m³, but extreme values are respectively 2767 et 3273 m³, i.e. -7.8 % and +9.1 % compared to the mean. In practice, this level of precision is acceptable. For time steps greater than 60 min, the dispersion increases dramatically and becomes more asymmetrical. For $\Delta t = 240$ min, the median is equal to 2532 m³ (-15.6 %) and extreme values are respectively 2399 m³ (-20.0 %) and 5718 m³ (+90.6 %).

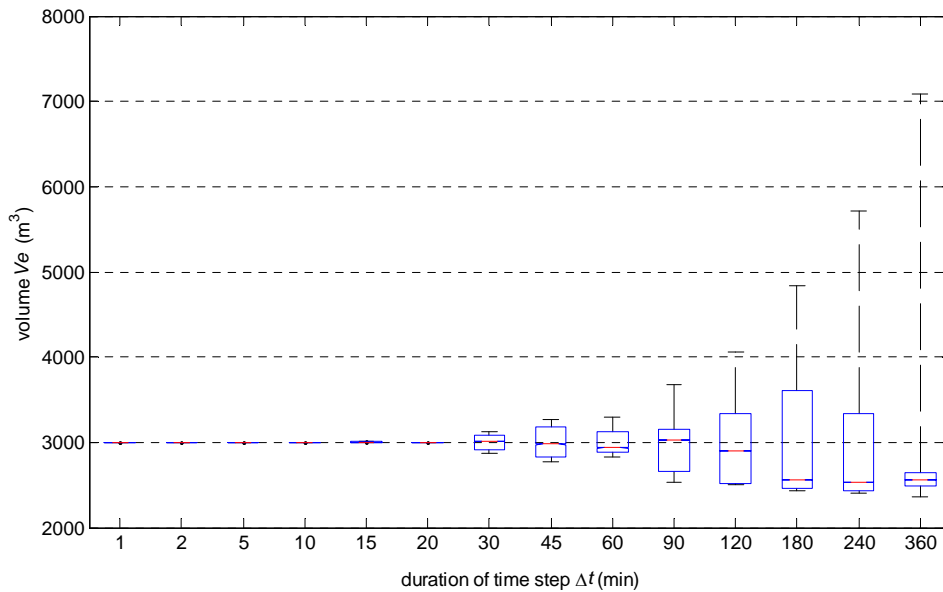


Figure 3.6: Effect of discretisation on the estimate $V_e(T)$

3.3.2.2 Effect of discretisation and random errors

In this second step, the discrete measured values are no longer considered as true values but are affected by random errors $e(t_j)$ sampled from normal distributions with mean values equal to zero and standard deviations equal to 7.5 % of the true values $Q(t_j)$, i.e. $u(q(t_j)) = 0.075 \times Q(t_j)$, as in section 3.3.1. Consequently, one calculates

$$V_e(T)_{si} = \left(\sum_{k=1}^{m_s} Q(t_{0si} + (k-1)\Delta t_s) \times (1 + 0.075 \times e_{sik}) \right) \Delta t_s \quad \text{eq. 37}$$

with e_{sik} the random error for $Q_{sik} = Q(t_{0si} + (k-1)\Delta t_s)$.

Five millions ($N = 5 \times 10^6$) simulations have been run to ensure stable boundaries of the 95 % coverage intervals for all values of Δt . Results are shown in Figure 3.7. Mean values, standard deviations and shortest 95 % coverage intervals of $V_e(T)$ are given in Table 3.3.

Compared to the previous step (discretisation only), standard deviations slightly increase due to random errors in measured values. For time steps of less than 20 min, uncertainty due to discretisation is either negligible or very low and the uncertainty due to random errors is the most important contribution to the uncertainty in $V_e(T)$.

However, the 95 % coverage intervals are very narrow (maximum ± 2 % of the mean value). For time steps equal to or greater than 30 min, the discretisation is the most important source of uncertainty in $V_e(T)$. When the time step increases, m_s decreases and the contribution of random errors in a decreasing number of measured values increases in absolute value. But this increasing contribution to the total uncertainty in $V_e(T)$ increases less rapidly, relatively, than the contribution due to the discretisation.

In Table 3.3 column E, the line corresponding to $\Delta t = 30$ min indicates that $u(V_e(T)) = 99$ m³. This value is similar to the standard uncertainty of 98 m³ calculated by means of the type B approach in section 3.3.1. The 95 % coverage interval in column F is [2827; 3170], to be compared with is [2771; 3163] obtained in section 3.3.1: both intervals can be considered equivalent (difference in lower and upper boundaries are resp. -2 % and -0.2 % with the interval in column F as the reference interval). However, it appears that 95 % confidence intervals calculated with the type B approach and the 95 % coverage intervals calculated with MC simulations will no longer be equivalent when Δt increases, because of the asymmetrical distribution of $V_e(T)$. In this case, MC simulations are a better and less biased approach.

The MC method illustrated in this section for the calculation of a cumulated volume will be further developed for a more critical issue: the calculation of pollutant loads when discrete samples are taken in sewer systems for laboratory analyses. Discrete sampling strategies will be compared to on line continuous measurements (e.g. turbidity) collected with short time steps (e.g. 2 minutes): in this case, on line water quality time series will be considered as the true reference signal and uncertainties due to both discrete sampling and laboratory analyses will be assessed.

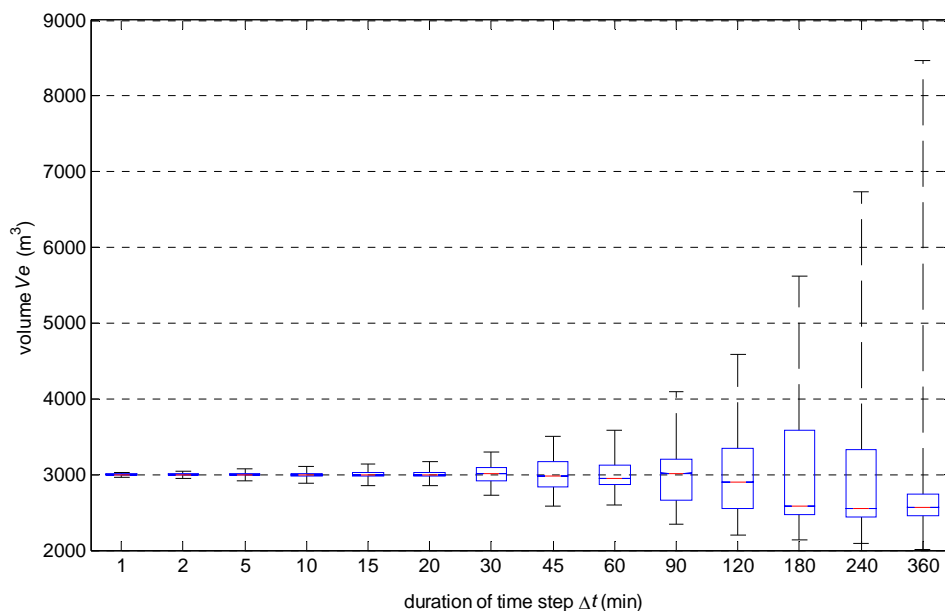


Figure 3.7: Effect of both discretisation and random errors on the estimate $V_e(T)$

Table 3.3: Standard uncertainties in $V_e(T)$ for two cases: i) with discretisation only (columns A to C), ii) with both discretisation and random errors (columns D to F)

| Δt (min) | discretisation only | | | discretisation + random errors | | |
|---------------------|--|---|-------------------------------------|--|---|-------------------------------------|
| | (A) mean $V_e(T)$ (m ³) | (B) $u(V_e(T))$ (m ³) | (C) 95 % coverage interval | (D) mean $V_e(T)$ (m ³) | (E) $u(V_e(T))$ (m ³) | (F) 95 % coverage interval |
| 1 | 3000 | $< 10^{-10}$ | [3000; 3000] | 3000 | 7.6 | [2985; 3015] |
| 2 | 3000 | $< 10^{-10}$ | [3000; 3000] | 3000 | 10.7 | [2979; 3021] |
| 5 | 3000 | $< 10^{-10}$ | [3000; 3000] | 3000 | 17 | [2967; 3033] |
| 10 | 3000 | $< 10^{-10}$ | [3000; 3000] | 3000 | 24 | [2953; 3047] |
| 15 | 3000 | 6 | [2993; 3009] | 3000 | 30 | [2941; 3059] |
| 20 | 3000 | $< 10^{-10}$ | [3000; 3000] | 3000 | 34 | [2933; 3066] |
| 30 | 3000 | 90 | [2867; 3120] | 3000 | 99 | [2827; 3170] |
| 45 | 3000 | 178 | [2767; 3269] | 3000 | 185 | [2723; 3317] |
| 60 | 2999 | 154 | [2833; 3292] | 3000 | 165 | [2767; 3338] |
| 90 | 3000 | 350 | [2534; 3646] | 3000 | 357 | [2456; 3672] |
| 120 | 3000 | 494 | [2500; 3993] | 3000 | 501 | [2388; 3999] |
| 180 | 3000 | 721 | [2427; 4621] | 3000 | 728 | [2277; 4606] |
| 240 | 2999 | 904 | [2399; 5205] | 3000 | 911 | [2208; 5192] |
| 360 | 3000 | 1082 | [2360; 5533] | 3000 | 1092 | [2143; 5569] |

3.4 APPENDIX TO EXAMPLE 1

3.4.1 Estimation of standard uncertainties in R , h and U

Note: the calculations presented in this section are only given as additional information in order to illustrate how various approaches can be used in uncertainty assessment. Other and/or improved approaches can also be applied.

3.4.2 Uncertainty in R

As it is easier in practice to measure the pipe diameter, the pipe radius R has been calculated from $n = 4$ measurements of the diameter D carried out at various positions in the pipe cross section, as given in Table 3.4.

Table 3.4: Four measurements of the pipe diameter

| |
|----------|
| D (mm) |
| 1002 |
| 1000 |
| 997 |
| 1002 |

The mean value $\bar{D} \approx 1000.25$ mm and thus the mean radius $R = \bar{D}/2 = 500.125 \approx 500$ mm. The standard deviation s of the four values of D is equal to 2.3629 mm. The 95 % confidence interval (with $\alpha = 0.05$) for the mean value \bar{D} is given by

$$\bar{D} - t_{1-\alpha/2}(v) \frac{s}{\sqrt{n}} \leq \bar{D} \leq \bar{D} + t_{1-\alpha/2}(v) \frac{s}{\sqrt{n}} \quad \text{eq. 38}$$

where t is the Student value for $v = n-1 = 3$ degrees of freedom: $t = 3.1824$.

Assuming that the above 95 % confidence interval can be re-written

$$\bar{D} - 2u(\bar{D}) \leq \bar{D} \leq \bar{D} + 2u(\bar{D}) \quad \text{eq. 39}$$

the standard uncertainty $u(D)$ is determined by

$$u(\bar{D}) = \frac{1}{2} \left(t_{1-\alpha/2}(v) \frac{s}{\sqrt{n}} \right) \approx \frac{1}{2} \left(3.1824 \frac{2.3629}{\sqrt{4}} \right) = 1.8799 \text{ mm} \approx 2 \text{ mm.} \quad \text{eq. 40}$$

Then $u(R) = u(\bar{D})/2 = 0.9399 \text{ mm} \approx 1 \text{ mm}$.

For calculations in this paper, one uses $R = 0.5 \text{ m}$ and $u(R) = 0.001 \text{ m}$.

3.4.3 Uncertainty in h

The water level h has been measured with a 0-2 m piezoresistive sensor. The sensor was previously calibrated in the laboratory. Details are presented in Bertrand-Krajewski and Muste (2007): only key results are given in this appendix. Reference water levels have been measured in a Perspex column (height 3.5 m, diameter 0.2 m) with a class II certified 4 m long metallic meter, with a standard uncertainty less than 0.5 mm. For each reference water level, considered as a standard value, 12 repeated measurements have been made with the piezoresistive sensor. The data are given in Table 3.5.

Table 3.5: Piezoresistive sensor calibration data. x_i = reference value, y_{ik} = repeated measurements with $k = 1:12$, $y_i \text{ mean}$ and s_i = respectively mean value and standard deviation of the 12 y_{ik} values. All values in mm

| x_i | y_{i1} | y_{i2} | y_{i3} | y_{i4} | y_{i5} | y_{i6} | y_{i7} | y_{i8} | y_{i9} | y_{i10} | y_{i11} | y_{i12} | $y_i \text{ mean}$ | s_i |
|-------|----------|----------|----------|----------|----------|----------|----------|----------|----------|-----------|-----------|-----------|--------------------|--------|
| 399 | 399 | 400 | 400 | 400 | 400 | 400 | 400 | 399 | 399 | 399 | 399 | 399 | 399.50 | 0.5222 |
| 799 | 800 | 800 | 800 | 800 | 800 | 800 | 800 | 800 | 800 | 800 | 800 | 800 | 800.00 | 0.0000 |
| 1200 | 1201 | 1201 | 1202 | 1202 | 1202 | 1202 | 1201 | 1201 | 1201 | 1201 | 1201 | 1201 | 1201.33 | 0.4924 |
| 1600 | 1601 | 1601 | 1601 | 1601 | 1601 | 1602 | 1600 | 1600 | 1600 | 1600 | 1600 | 1600 | 1600.58 | 0.6686 |
| 2000 | 2002 | 2002 | 2002 | 2002 | 2002 | 2002 | 2001 | 2001 | 2001 | 2001 | 2001 | 2001 | 2001.50 | 0.5222 |

Ordinary least squares regressions have been made and compared by means of F-tests. The resulting optimal calibration function, with a residual variance $s_f^2 = 0.344398$, is

$$y = a + bx = 0.508854 + 1.000395 x \quad \text{eq. 41}$$

It is then possible to transform any measured value y_0 into the corresponding most likely true value of the water level x_0 , and also to evaluate its standard uncertainty $u(x_0)$. Consider one single measured value $y_0 = 701 \text{ mm}$. The most likely true value x_0 is calculated with eq. 42:

$$x_0 = \frac{y_0 - a}{b} = \frac{701 - 0.508854}{1.000395} \approx 700.2 \text{ mm} \quad \text{eq. 42}$$

The standard deviation $s(x_0)$ is due to two independent contributions: i) the uncertainty in the measured value y_0 , and ii) the uncertainty in the calibration curve expressed by the uncertainties in both coefficients $s(a)$ and $s(b)$. $s(x_0)$ is calculated by:

$$s(x_0)^2 = \frac{s_f^2}{b^2} \left(1 + \frac{1}{N} + \frac{(x_0 - \bar{x})^2}{\sum_i n_i (x_i - \bar{x})^2} \right) = \frac{0.344397}{(1.000395)^2} \left(\frac{61}{60} + \frac{(700.2 - 1199.6)^2}{19228814.4} \right) = 0.3543 \quad \text{eq. 43}$$

Accordingly, adopting $u(x_0) = s(x_0)$ produces $u(x_0) \approx 0.6 \text{ mm}$. The 95 % confidence interval (enlargement factor equal to 2) for x_0 is then given by $[x_0 - 2u(x_0), x_0 + 2u(x_0)] \approx [699.0, 700.4]$. The final result is expressed $x_0 = 700.2 \pm 1.2 \text{ mm}$.

The above result means that the sensor standard uncertainty, for $y = 700 \text{ mm}$, is equal to 0.6 mm, under stable laboratory or calibration conditions.

However, in the field (e.g. in a real sewer), the *in situ* measurement standard uncertainty is greater than 0.6 mm because the water level is not perfectly flat and stable but uneven with at least small waves, the free surface is

not strictly horizontal due to turbulence and secondary flows, the exact position of the sensor in the pipe section is not known with a very high precision, etc. An *empirical global estimate* of this additional sources of uncertainty, *based on visual observations* made in various measurement locations in sewers, is evaluated to be about $u_r = 5$ mm (see e.g. Bertrand-Krajewski *et al.*, 2000, p. 223). In some cases, the above small deviations from flat free surface could be more significant, leading to significant biases and errors, and it may be necessary e.g. to use a set of sensors instead of a unique one to estimate the average water level. Nevertheless, too complex hydraulic conditions shall be avoided for flow measurements: alternative locations and even local reconstruction or modification of the infrastructure may be necessary. A special attention to local hydraulic conditions, sewer geometry, sensor location, and to resulting errors and uncertainties is mandatory.

As a consequence of the above indication for this example, the *in situ* measurement standard uncertainty $u(h)$, with the above sensor, is assumed to be equal to

$$u(h) = \sqrt{u(x0)^2 + u_r^2} = \sqrt{0.6^2 + 5^2} = \sqrt{0.36 + 25} \approx 5 \text{ mm} \quad \text{eq. 44}$$

For calculations in this paper, one uses $h = 0.7$ m and $u(h) = 0.005$ m.

During storm events and high flows, based on *in situ visual* observations, $u(h)$ may be higher, up to 15 mm. This indicates clearly that, if the water level sensor is of good quality with low uncertainties, the main source of uncertainty for *in situ* measurement is due to the natural turbulence and instabilities of water surfaces.

If detailed information is available, it could be possible to propose a simple empirical function to estimate $u(h)$ as a function of h or of the discharge Q .

3.4.4 Uncertainty in U

The mean flow velocity U is calculated from the information provided by the Doppler sensor. The Doppler sensor, when located on the pipe invert, is determining the mean velocity V (m/s) within a conical volume characterised by three parameters: its angle of inclination related to the horizontal line, its angle of aperture, and its length. The two first parameters are given in manufacturer's specifications. The length, which determines the volume explored by the sensor, is not fixed and depends on factors like e.g. the variable suspended solids concentration or the ultrasound emission frequency. As the sensor explores the conical volume which is only a fraction of the cross-section, and as velocity profiles are not uniform through the cross section, the mean velocity U (m/s) through the cross section is usually calculated by $U = kV$, where k is a correction factor to account for geometry, flow regime, velocity profiles, etc.

Theoretically, $u(U)$ could be evaluated from $u(V)$ and $u(k)$ and by using the law of propagation of uncertainties. In practice, this is much more complex, as $u(V)$ and $u(k)$ are not known and difficult to assess. On the one hand, $u(V)$ is not constant and depends on the discharge conditions (pipe geometry, flow regime, depth of flow, etc.). Manufacturers may provide some values for $u(V)$, but they are only indicative and do not necessarily correspond to real conditions of use in sewers. Indeed, in most cases, they are estimated either i) by moving the sensor with a known velocity over a basin with still water, like for calibration of propeller velocity meters, which does not correspond to realistic vertical velocity profiles (see Bertrand-Krajewski *et al.*, 2000, p. 371), or ii) by doing measurements under controlled laboratory conditions for limited circular pipe conditions with clean water, which cannot be transposed to real sewers. On the other hand, k also changes with flow conditions (geometry, depth of flow, etc.) and estimating its uncertainty means that one has another and more precise method to estimate the discharge. These difficulties led us to use a more conservative and empirical approach.

A first attempt consisted to compare, in a real sewer, the mean velocity along a vertical profile measured with a calibrated propeller velocity meter and the mean velocity V given by a floating Doppler sensor oriented toward the pipe invert (Bertrand-Krajewski *et al.*, 2000, p. 374). Such experiments have been repeated later on (unpublished results) with a calibrated punctual electromagnetic velocity meter OTT Nautilus C2000. As these measurements are time consuming and cannot be easily carried out and repeated under various flow conditions in sewers, we concluded that, as an empirical conservative first approximation, $u(U)$ is around 0.05 m/s, for some circular or egg-shape man-entry sewers, and only for water levels between 0.15 and 0.4-0.5 m (for security reasons, it is not possible to carry out measurements in sewers with higher water levels occurring during storm events).

Obtaining more accurate *in situ* estimations of $u(U)$ requires independent, reliable and precise discharge measurements. More recently, we applied both salt and Rhodamine WT repeated tracing experiments, with one second time step continuous measurements of electric conductivity and fluorescence respectively, with calibrated

sensors. These experiments may provide measurements of the discharge Q with an enlarged uncertainty of less 6 % (preliminary results are given in Lepot *et al.*, 2010). Knowing Q and the water level h also measured during the tracing experiments, one can then derive U and its uncertainty. Repeated tracer experiments for various water levels and flow conditions will allow better estimating of $u(U)$ than the previous comparisons with velocity meters.

3.4.5 Matlab source code for MC calculations

```
R = 0.5 + 0.001*randn(1e6,1);
h = 0.7 + 0.005*randn(1e6,1);
U = 0.8 + 0.05*randn(1e6,1);
Q = R.^2.*(acos(1-h./R)-(1-h./R).*sin(acos(1-h./R))).*U;
result = IC95min(Q)
```

with IC95min the following function

```
function y = IC95min(V)
% this function gives a horizontal vector y = [m p1 p2]
% with m the mean value and p1 and p2 the boundaries of the shortest
% 95% coverage interval of the vector V
j = (0:0.01:5)';
m = prctile(V,j+95)-prctile(V,j);
[~, b]=min(m);
y = [mean(V) prctile(V,j(b)) prctile(V,j(b)+95)];
```

4. EXAMPLE 2: ESTIMATION OF TSS AND COD POLLUTANT LOADS FROM CONTINUOUS TURBIDITY MEASUREMENTS IN TWO URBAN SEWER SYSTEMS

4.1 INTRODUCTION

This example is less detailed in terms of algebra and calculations compared to the previous example, as they are similar in their principle, but more complete in terms of application and operational results. It presents some key methodological aspects for continuous data acquisition and data processing. Their application is illustrated for two experimental urban catchments in Lyon, France: i) Chassieu, 185 ha, industrial area with a stormwater separate system, ii) Ecully, 245 ha, residential area with a combined system, respectively with 263 and 239 storm events recorded (rainfall, discharge, turbidity time series) in the period 2004-2008 with a 2 minute time step. This example is copied, with very minor modifications, from Bertrand-Krajewski and Métadier (2010).

The methodology includes the following main steps:

1. calibration of sensors and determination of calibration functions
2. data correction and estimation of uncertainties in corrected data
3. automated data pre-validation by application of a set of parametric tests
4. final data validation by an operator
5. calculation of discharge, TSS and COD concentrations, and their uncertainties
6. calculation of storm event TSS and COD loads and of their uncertainties, including the dry weather contributions in case of a combined sewer system.

Steps 1 to 4 have been previously described in other papers (see Métadier and Bertrand-Krajewski, 2011). Steps 5 and 6 are briefly presented in the following paragraphs.

4.2 CALCULATION OF DISCHARGE AND CONCENTRATIONS OF TSS AND COD

Various methods can be used to calculate discharge including: (i) Manning-Strickler applied to water level, (ii) a water level-velocity relationship in cases where it is locally known, (iii) a locally established rating curve or (iv) a combination of water level and flow velocity measurements. Standard uncertainties in discharge can be calculated by means of the GUM or MCM approaches. TSS and COD concentrations are calculated from correlation functions for turbidity, for both dry and wet weather periods. Correlation functions are determined either by the ordinary least squares regression or the Williamson regression, preferably. Details are given in Bertrand-Krajewski *et al.* (2007) and Torres (2008).

4.2.1 Event load calculation

TSS and COD event loads are calculated with their standard uncertainties. This includes two sub-steps which are described hereafter: (i) the automated determination of the duration of the hydrologic event and (ii) the calculation of the event load itself between the determined storm event limits.

The duration of the hydrologic event comprises (i) the storm event duration itself, i.e. the time between the beginning and the end of the rainfall event as measured with the rain gauge and ii) the time needed for a set of variables (discharge, conductivity, turbidity) to reach again the values they had before the storm event started. The identification of the beginning t_d and the end t_f of hydrologic events is based on 3 criteria: (i) discharge threshold, (ii) minimum period between 2 successive independent events and (iii) the maximum duration between the beginning of the storm event and the rising of the discharge in the sewer. The identification of the end of hydrologic events is more complex than the identification of the beginning as, in some cases, pre-event dry weather values of conductivity and/or turbidity are not reached again even many hours after the end of the rainfall event.

Event loads are calculated by integration over the storm event duration of the continuous discharge and TSS or COD concentration time series:

$$M_X = \left(\sum_{i=1}^N C_{Xi} Q_i \right) \Delta t \quad \text{eq. 45}$$

where M_X is the event load of pollutant X (kg), C_{X_i} is the concentration of pollutant X (kg/m³) at time step i , Q_i is the discharge (m³/s) at time step i , Δt is the duration (s) of the time step, i is the index, and N is the number of time steps corresponding to the duration of the hydrologic event: $N = (t_f - t_d)/\Delta t$.

Standard uncertainties in TSS and COD pollutant loads are calculated by means of the LPU taking into account discharge and concentration uncertainties.

4.2.2 Determination of dry weather contribution during storm events

Most models of storm weather pollutant loads in combined sewer systems are based on the assumption that the total storm event load is the sum of i) the DW (dry weather) contribution that would have been observed during the event duration if no event had occurred and ii) the WW (wet weather) contribution including surface runoff + possible erosion of deposits accumulated in the sewers. The DW contribution during a storm event can be estimated from turbidity time series.

In addition to eq. 45, it is assumed that:

$$M_X = M_{X_DW} + M_{X_WW} \quad \text{eq. 46}$$

$$V = V_{DW} + V_{WW} \quad \text{eq. 47}$$

with M_{X_DW} the DW contribution, M_{X_WW} the WW contribution to the total mass M_X , V the total event volume, V_{DW} the DW volume during the storm event and V_{WW} the WW volume generated by the storm event.

M_{X_DW} is the pollutant load that would have been measured if no storm event had occurred: by definition, it cannot be measured and should be estimated. The proposed method to estimate M_{X_DW} consists to determine the most likely DW discharge and turbidity time series (i.e. DW signals) compatible with the DW time series measured after and before the observed storm event. This most likely DW signal, named hereafter the reference signal, is chosen among available measured DW days which are close to the day during which the storm event occurs. The two steps are the following ones: i) test of several DW signals by juxtaposing them to the storm event signal and ii) comparing the values and the dynamics of the two signals on common DW periods of some hours on both sides (before and after) of the storm event limits: these periods are named the fitting periods. The DW signal having the most similar dynamics over the fitting periods is selected to estimate M_{X_DW} . In other words, it is assumed that if a tested DW signal is similar to the DW signal measured before and after the considered storm event, it is also an appropriate estimation of the un-measurable DW signal during the storm event. Possible alternative solutions to the above data base analysis include e.g. dry weather forecasting techniques, with a specific analysis of uncertainties.

The method is illustrated Figure 4.1, where four signals (fitting periods) A to D (dotted lines) are compared with the dry periods before and after a storm event. The most similar signal over the fitting periods is signal C, which is consequently applied to estimate the DW signal during the storm event. This approach is used for both discharge Q and turbidity T signals.

The DW signals to be tested are not chosen randomly but according to a pre-established DW days classification (see paragraph 4.4). The selected reference signal shall satisfy the following criteria: i) both discharge and turbidity series are available without any gaps, ii) it must be long enough over the fitting periods to ensure a reliable comparison, iii) it is not necessarily an entire DW day as long as the fitting periods are fully covered and iv) it can be composed of several DW days in case the storm event is occurring over more than one day (e.g. weekdays and weekends).

In case reference and measured signals are comparable over the fitting periods in terms of dynamics but not in terms of absolute values, the reference signal can be translated by applying a simple mathematical signal fitting, independently for discharge and turbidity. It is based on a least squares minimization of the distance between the two signals, by ignoring extreme distances that correspond to random peaks (especially for turbidity). As for dynamics comparison over the fitting periods, the need for translation is visually evaluated by the operator, with some possible degree of subjectivity. However, based on our experience with long continuous time series, the reference signal translation is rarely required, given measurements from rather close DWDs are usually available. The fitting may be necessary in case of long term gaps in the continuous series or long rain periods, for which no adequate DW periods are available.

M_{X_DW} is then calculated from the reference signal at each time step i during the storm event duration:

$$M_{X_DW} = \Delta t \cdot \sum_{i=t_d_DW}^{t_f_DW} C_{Xi_DW} \cdot Q_{i_DW} \quad \text{eq. 48}$$

with Q_{i_DW} the reference signal discharge, C_{Xi_DW} the reference signal concentration of pollutant X computed from the signal reference turbidity $Turb_{i_DW}$, and t_d_DW and t_f_DW the reference signal starting and ending times corresponding to the storm event limits t_d and t_f .

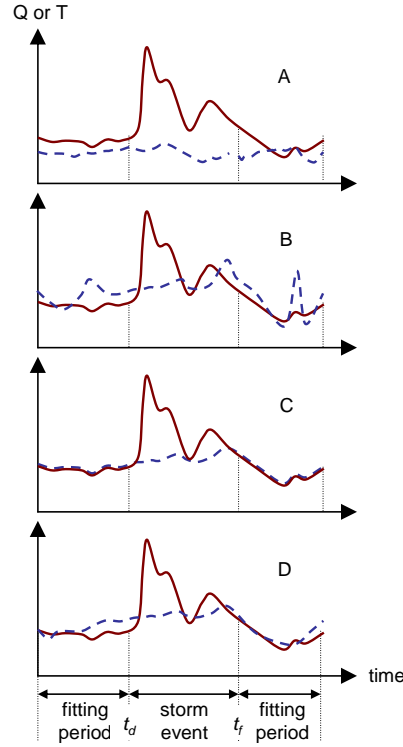


Figure 4.1: Example of estimation of the most-likely dry weather contribution during a storm event

The standard uncertainty $u(M_{X_DW})$ is then calculated by means of the LPU:

$$u(M_{X_DW})^2 = \Delta t^2 \left(\sum_{i=t_d_DW}^{t_f_DW} Q_{i_DW}^2 \cdot u(C_{Xi_DW})^2 + C_{Xi_DW}^2 \cdot u(Q_{i_DW})^2 \right) \quad \text{eq. 49}$$

with $u(C_{Qi_DW})$ and $u(C_{Xi_DW})$ the standard uncertainties at time step i resp. for discharge and concentration of pollutant X of the reference signal.

Compared to total event load uncertainty, the DW contribution uncertainty includes an additional source of uncertainty which is related to the DW contribution estimation method itself, *i.e.* the error due to the fact that the reference signal is substituted to the true but unknown DW signal. Thus, the uncertainty of the substituted discharge and turbidity signals at each time step i of the signal reference include both the measurement uncertainty $u(Q_{i_DW_m})$ and $u(Turb_{i_DW_m})$ and a substitution uncertainty $u(Q_{i_DW_subs})$ and $u(Turb_{i_DW_subs})$. Under the assumption that substitution uncertainties are normally distributed:

$$u(Q_{i_DW})^2 = u(Q_{i_DW_m})^2 + u(Q_{i_DW_subs})^2 \quad \text{eq. 50}$$

$$u(Turb_{i_DW})^2 = u(Turb_{i_DW_m})^2 + u(Turb_{i_DW_subs})^2 \quad \text{eq. 51}$$

More details about uncertainties in substituted values are given in Métadier and Bertrand-Krajewski (2010b).

4.3 APPLICATION TO THE CHASSIEU CATCHMENT WITH A SEPARATE SEWER SYSTEM

The above methodology has been applied to the 185 ha Chassieu catchment. It is drained by a separate stormwater sewer system which has sensors at its outfall sewer to continuously monitor water level and water quality indicators (turbidity, conductivity, pH and temperature) with a 2 minutes time step. Water quality indicators are not measured directly in the sewer but in a monitoring flume continuously supplied by a 1 L/s peristaltic pump. Five years of data have been collected for the period 2004 -2008. All sensors are calibrated twice in a year. A variable variance was applied to turbidimeters because calibration tests revealed that the variance is significantly higher beyond 1000 NTU. *In situ* standard uncertainties have been estimated to be equal to 7.5 mm and 10 % of the measured value respectively for water level and turbidity values. For automatic event identification, data from the nearest rain gauge were used. Other criteria were set as follows: discharge threshold = 4 L/s, minimum duration between 2 successive events = 4 hours, maximum duration between beginning of storm event and rising discharge = 6 hours.

Figure 4.2a and Figure 4.2b shows respectively the Turbidity-TSS (left figure) and Turbidity-COD (right figure) correlation functions for wet weather conditions. Both are second order polynomial functions determined by means of Williamson regression to account for uncertainties in both variables (turbidity and TSS or COD). Grey areas correspond to 95 % confidence intervals in estimated TSS or COD concentrations. It is important to note that both functions have been established with samples collected during various storm events covering a large measurement range (respectively 0 - 680 NTU corresponding to 0 - 1000 mg/L of TSS and 0 - 800 NTU corresponding to 0 - 800 mg/L of COD). This is important to ensure that the correlation functions are applicable for various conditions and without undue extrapolation.

In 2005, 33 storm events have been monitored in Chassieu. For each event, TSS and COD event loads have been calculated, with their 95 % confidence intervals. The results are shown in Figure 4.2c: black and white thick bars represent respectively the TSS and COD loads for the 33 events. Each thick bar is completed with a vertical thin bar segment representing the 95 % confidence interval of the event load. The variability of the event loads is very significant, with values ranging typically from quite small to 400-500 kg of TSS or COD per event. The event number 25 shows extremely high loads compared to all the other ones. A further analysis of these 33 events loads (results not shown here) has indicated that there was no correlation between events loads and basic event characteristics like rainfall duration, intensity, and antecedent dry weather period or rainfall return period.

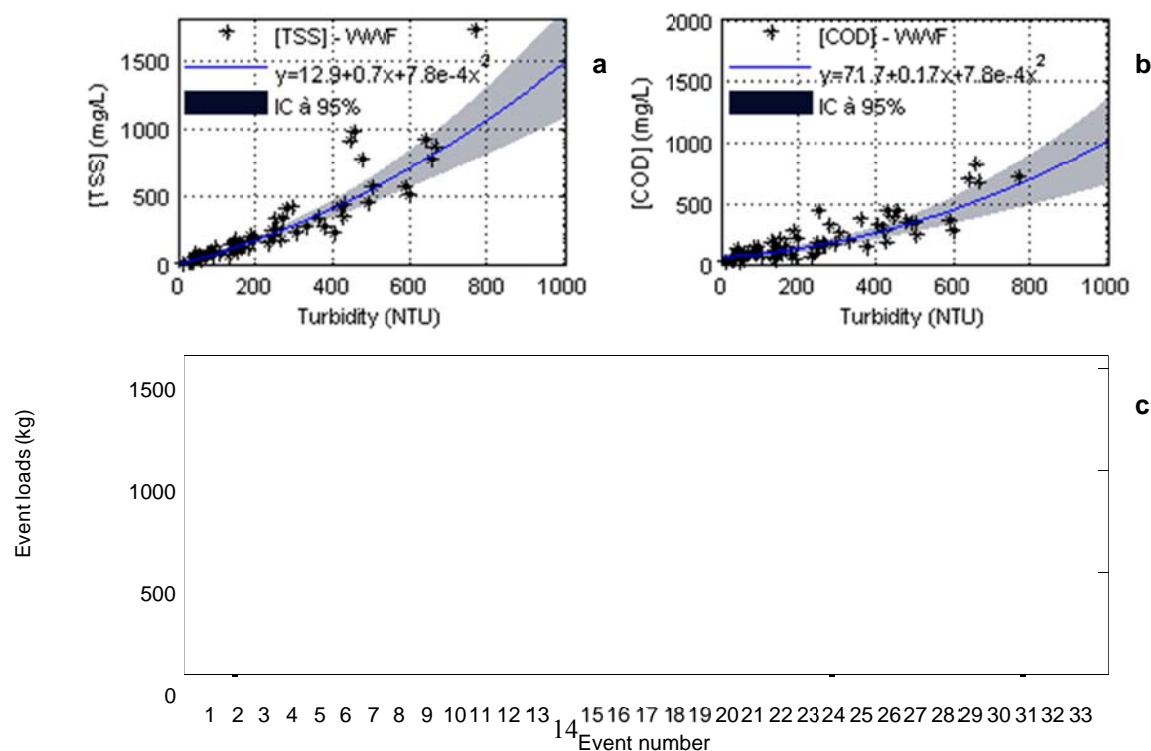


Figure 4.2: Example of results for the Chassieu catchment: (a) Turbidity-TSS and (b) Turbidity-COD correlation functions, (c) TSS (in black) and COD (in white) event loads in 2005 with 95 % coverage intervals

4.4 APPLICATION TO THE ECULLY CATCHMENT WITH A COMBINED SEWER SYSTEM

The methodology has also been applied to the 245 ha Ecully catchment drained by a combined sewer system. Three clearly distinct DW daily pattern classes were identified among the available 180 DW days recorded in 2007-2008: i) class 1: weekdays (Monday to Friday) without school holidays, ii) class 2: weekends (Saturday and Sunday) and weekdays with general public holidays and iii) class 3: weekdays (Monday to Friday) with school holidays. The three classes represent respectively 55 %, 22 % and 23 % of the 180 DW days (resp. 99, 40 and 41 DW days). The three classes correspond to calendar percentages over the period 2007-2008 of 41, 32 and 32 %, evidencing a satisfactory representativeness of the available DW data. In order to analyse the DW pattern variability, mean discharge and turbidity profiles for the period 2007-2008 were computed for each class and for all classes together, with standard deviations and coefficients of variation computed at each time step of the profiles (720 values per day). 5 % - 95 % percentile intervals and distributions of residuals (distances from the each DW day value to the mean profile) were also computed. Results are summarised in Table 4.1 and illustrated in Figure 4.3 and Figure 4.4 resp. for class 2 and for all classes together (named hereafter class 4).

The results are rather similar for all classes. Residuals are approximately log-normally distributed. The computed 5 % - 95 % percentile intervals are comparable for the four classes, with larger values for high flow periods around 10:00-12:00. Dispersion is significantly higher for turbidity with mean coefficients of variation around 30-35 % compared to 20-25 % for discharge. Moreover 5 % - 95 % percentile intervals are less smoothed for turbidity, which is explained by the random turbidity peaks observed during the day especially during high flow period at the end of morning and evening peaks. This trend is even more pronounced when results are analysed at 2 min time step. Comparable orders of magnitude of the variability for both discharge and turbidity signals have been observed by Lacour (2009) in two urban combined catchments in Paris, France.

Table 4.1: Mean standard deviations and mean coefficients of variation of the mean discharge and turbidity along the DW profiles for classes 1 to 4

| Class | Mean standard deviation | | Mean coefficient of variation | |
|---------|-------------------------|-----------------|-------------------------------|---------------|
| | Discharge (L/s) | Turbidity (NTU) | Discharge (%) | Turbidity (%) |
| Class 1 | 7.05 | 55.23 | 21.86 | 31.80 |
| Class 2 | 6.52 | 51.31 | 22.69 | 29.25 |
| Class 3 | 9.46 | 59.33 | 28.6 | 36.39 |
| Class 4 | 7.91 | 60.18 | 23.75 | 34.66 |

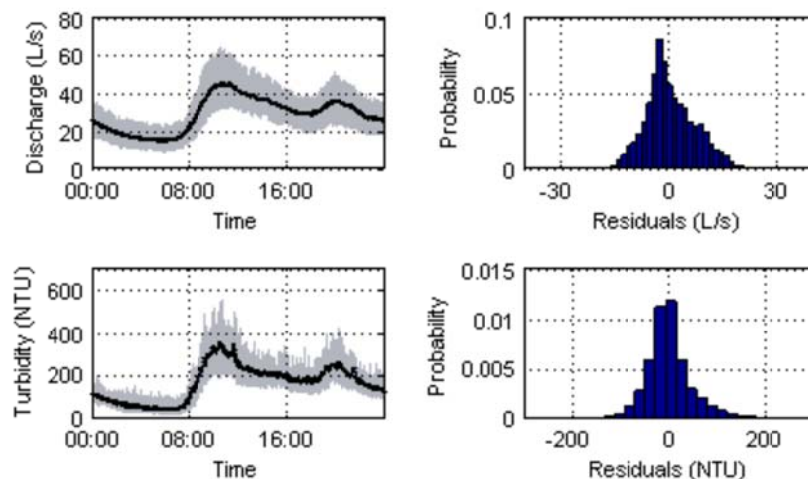


Figure 4.3: Class 2 mean DW discharge and turbidity patterns, with 5 % - 95 % percentiles interval (left) and residuals distribution (right)

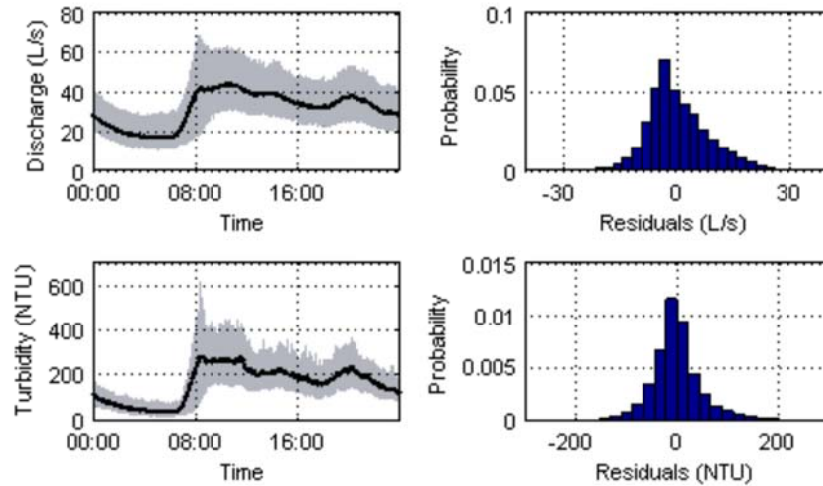


Figure 4.4: Class 4 mean DW discharge and turbidity patterns, with 5 % - 95 % percentiles interval (left) and residuals distribution (right)

TSS and COD event loads calculation have been calculated for the 239 storm events measured in Ecully in 2007-2008. Constant substitution uncertainties were applied, respectively equal to 3.33 L/s and 47.0 NTU for discharge and turbidity. As an example, Figure 4.5 illustrates the storm event dated Friday 31 October 2008, which is a class 3 DW day. The rainfall depth is 10.7 mm. Event starting and ending times are respectively 12:28 and 20:28. The selected reference signal corresponds to Tuesday 4 December 2008, which is available in the DW data base. The left graphs represent, from top to bottom, the rainfall intensity, the conductivity, the discharge and turbidity reference signals measured on Tuesday 4 December 2008, and the measured discharge and turbidity signals measured on Friday 31 October 2008. The right graphs represent, from bottom to top, COD and TSS mass fluxes (in kg/s) computed from the TSS-turbidity and COD-turbidity correlations, and event pollutant loads with the black, grey and white bars representing respectively the total event loads, the wet weather load contribution and the dry weather load contributions (in kg). For discharge, turbidity, fluxes and event loads, 95 % confidence intervals are computed with the LPU. Event runoff volume, TSS and COD loads with WW and DW contributions and their 95 % confidence intervals are summarized in Table 4.2.

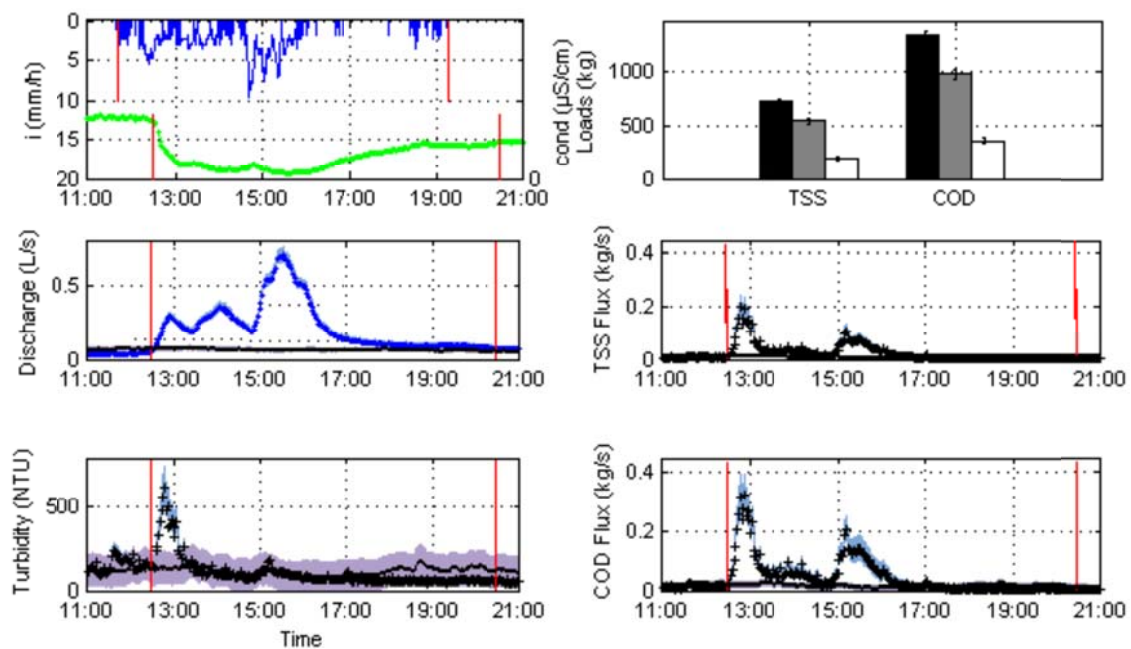


Figure 4.5: Illustration of the methodology for the storm event dated 31 October 2008

Table 4.2: Results for the storm event dated Friday 31 October 2008

| Friday 31 Oct. 2008 | Total | WW contribution | DW contribution |
|---------------------|----------------------------|----------------------------|----------------------------|
| Runoff | 6323 +/- 26 m ³ | 4645 +/- 62 m ³ | 1718 +/- 32 m ³ |
| TSS load | 729 +/- 22 kg | 540 +/- 26 kg | 189 +/- 13 kg |
| COD load | 1324 +/- 42 kg | 967 +/- 46 kg | 356 +/- 20 kg |

5. EXAMPLE 3: UNCERTAINTY EVALUATION OF MULTI-SENSOR FLOW MEASUREMENT IN A SEWER SYSTEM USING MONTE CARLO METHOD

The following case study is a more detailed example of application of MCM to discharge measurements in a sewer system. The MCM is used hereafter to carry out the evaluation of the measurement uncertainty, considering its inherent capacity to deal with non-linear and multi-stage mathematical models. Influence of geometric conditions and other relevant parameters in the quality of measurements is discussed. The study was developed within the context of a specific sewer system, using a particular measurement system, from which measurement data was gathered. This example is copied, with very minor modifications, from Ribeiro *et al.* (2010).

5.1 INTRODUCTION

Measurement of flow in sewer systems is a complex task considering the dynamic behaviour of the measurand and the effects resulting from non-ideal conditions of operation (Larrarte, 2006). When flow measurements are regularly used for managing sewer systems, performance of the measurement system and the quality of measurement results becomes critical both to daily operation and to decision making processes within the utility.

Different solutions can be adopted in order to measure flow in free surface flow conditions in sewers (Bertrand-Krajewski *et al.*, 2000). One of the most common methods is the velocity-area, usually using multi-sensing flow meters composed by a combination of sensors for level and velocity measurement, often mounted in stainless steel rings or bands, to be fitted in the inner surface of sewer pipes. The flow can be calculated from measurement of different quantities, namely, level and velocity, by applying the continuity equation. The slope-area methods, using the Manning-Strickler formula or similar formulae, are sometimes used in conjunction with the velocity-area method to ensure redundancy. In both cases, calculation of the flow involves the use of non-linear mathematical models in a multi-stage system. Additionally, in general, these methods assume uniform flow conditions often difficult to ensure in actual measurement sites. For the purpose of this example, only the continuity equation is considered.

The development of the uncertainty budget requires the evaluation of contributions due to different uncertainty sources, which can be grouped in eight major factors: the measurand; the instrumentation metrological performance; the calibration; the sampling; the interface; the user; the environmental conditions; and the data processing.

In the specific case under study, considering the technological development of instrumentation and data processing software, the non-ideal conditions of the measurand realization (i.e. non-uniform flow) appears to be an important contribution.

The analysis of the instrumentation assembly and its installation *in situ* shows the relevance of a number of geometric requirements: the placement of probes, measuring angles and cross-sectional geometry. In addition, hydraulic conditions associated with the inner pipe characteristics (symmetry conditions, wall roughness, hydraulic jump, drops, curves and infrastructure irregularities) can generate different types of waves, energy losses and other disturbances contributing to non-uniform flow.

In order to study the sources of measurement uncertainties and their effects, a second aim of this example is to obtain an assessment of the conditions that make the contributions due to geometric quantities dominant in the context of the uncertainty budget.

5.2 METHODOLOGY

Flow is a quantity measured indirectly, usually obtained by the measurement of other quantities and applying mathematical models, the continuity equation being one of the most common. The continuity equation, as given by eq. 52, is a functional relation that yields the volumetric flow rate, Q , as a function of the mean velocity, U , and the cross sectional area of flow, A , according to the principle of conservation of mass.

$$Q = U \cdot A \quad \text{eq. 52}$$

In practice, the input quantities of this mathematical model, obtained by indirect measurement of other measurands, create a multi-stage metrological problem with several input and output quantities, and functional relations between them, to reach the final output measurand, Q .

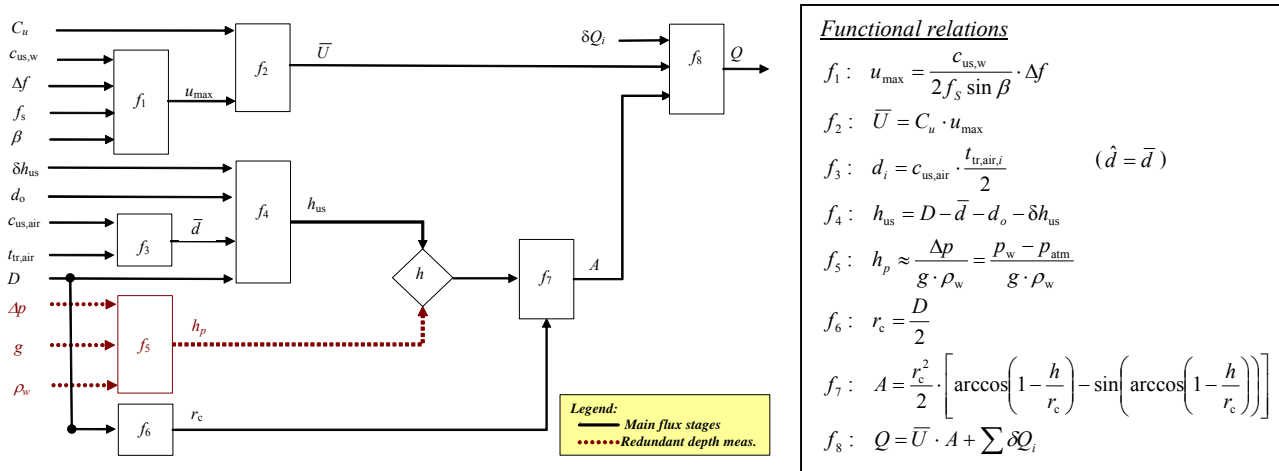


Figure 5.1: Input quantities and functional relations to obtain volumetric flow rate

Table 5.1: Set of quantities applied

| Symbol | Description |
|-------------------------|---|
| $c_{us,w}$ | Ultrasound velocity in water (at reference conditions) |
| f_s | Emitter frequency |
| β | Angle of sound propagation |
| Δf | Doppler frequency shift |
| u_{\max} | Peak flow velocity |
| C_u | Peak to average flow velocity factor |
| \bar{U} | Average flow velocity |
| $c_{us,air}$ | Ultrasound velocity in air (at reference conditions) |
| $t_{tr,air,i}$ | Wave time of transit |
| d_i, \hat{d}, \bar{d} | Displacement, estimate and average values |
| D | Diameter of pipe (at flow depth section measurement) |
| d_o | Displacement offset of the acoustic emitter |
| δh_{us} | Flow depth variation in the measurement surface |
| h_{us} | Flow depth (measured with acoustic us instrument) |
| p_w, p_{atm} | Pressure of fluid (water) and atmospheric pressure |
| g | Gravity |
| ρ_w | Density of water (at reference conditions) |
| h_p | Flow depth (measured with pressure depth instrument) |
| r_c | Radius of conduit (at the cross-section area) |
| A | Cross-section "wet" area |
| δQ_i | Flow influence quantities related with the method and with computational processing |
| Q | Volumetric flow rate |

The flow through a given surface S is defined as the result of an integration of a velocity field over that target surface. Thus, U is the average of the field velocities over S . The pattern of the velocity field spatial distribution may vary significantly according to the type of flow (e.g. in completely filled pipes or free surface flow) and local conditions. The best approximation to the average velocity U in a given flow should be obtained by measuring velocities in a large number of points distributed over the target surface, S .

The measurement of U is often carried out by transducers that capture the effect of the velocities along a straight line or, more realistically, along the conical dispersion of the beam (Edelhauser, 1999; Jaafar *et al.*, 2009), by assuming that certain flow distribution and symmetry conditions are well known and that yield feasible

solutions. Then, the average velocity U is obtained from a measured value (which can be either a beam average value or its maximum value) multiplied by an appropriate calibration factor.

The complexity of the relations established between quantities is presented in Figure 5.1, showing several stages where some quantities are simultaneously output of some stage and input to the next stage. The complete set of quantities used is described in Table 5.1, being based on the formulation presented in Figure 5.1.

The experimental performance of flow measurement in sewers implies that some influence quantities related to the method deviations, δQ_i , should additionally be taken into account in the mathematical model, as included in (f_8) . This modification of the mathematical model (eq. 52) is required in order to evaluate the measurement uncertainty. Both relations are in agreement if the average values of these quantities are null (as usually expected).

The random variable flow depth, h_{us} , can be estimated from two different measurement approaches (Doppler effect or fluid column pressure), allowing to have redundant information about system performance.

In order to test the proposed approach as a means for evaluating the flow measurement uncertainty, measurement data from a large sewer system were used. This regional sewer system has circa 60 flow measurement locations, and measurement accuracy constitutes an important issue since data is used for billing purposes. The measurement approach used in most locations is based on the velocity-area method and the cross-section shape on locations selected is circular (Figure 5.2 and Figure 5.3).

The information obtained allows to calculate estimates of the measurement uncertainty contributions and to discuss the model sensitivity to different parameters such as those related with the geometric conditions.



Figure 5.2: Flow measurement using the velocity-area method



Figure 5.3: Flow measurement device: detail of ultrasound device (four pairs) for flow depth measurement

In most of the measurement locations, mounting the instrumentation is made under adverse conditions, usually in places where flow performance can be strongly affected by the geometry of pipes and by irregularities in joints. Furthermore, in conditions where flow imposes strong impulses on the instrumentation, dislocations of the instrumentation supporting ring causes permanent changes in the setup, dragged objects and debris might damage the instrumentation, and sediment grease and oil accumulation can obstruct the sensors. These

unpredictable events eventually identified during maintenance operations or data processing, can lead to significant measurement errors. However, incorporation of these effects as contributions to measurement uncertainty proves to be difficult. Thus, it is expected that the error sources are strongly dependent of local conditions at each measurement location.

The evaluation of the measurement uncertainty contributions is based on the analysis of the variability of average values obtained from several locations. The probability distributions were derived from the observation of some variables during the measurement process, together with estimated values provided by the manufacturers or by referenced bibliography

5.3 EVALUATION OF MEASUREMENT UNCERTAINTY USING MCM

Regarding the process used by the Monte Carlo Method (MCM) to perform the evaluation of measurement uncertainties, the relations (mathematical models) of the multi-stage system are used directly, together with the input data obtained by sampling from probability density functions (PDFs) of each input quantity. The computation of the algorithm gives the propagation of distributions in order to obtain the output quantities PDFs and their statistical parameters of interest (namely, measurands best estimates and variances).

The propagation of PDFs from one stage to the following is illustrated in Figure 5.4, assuming that the output numerical sequence of one stage (with its own PDF) is taken as the input numerical sequence of the next stage, while keeping the statistical properties (such as correlations) characteristic of the each specific random variable.

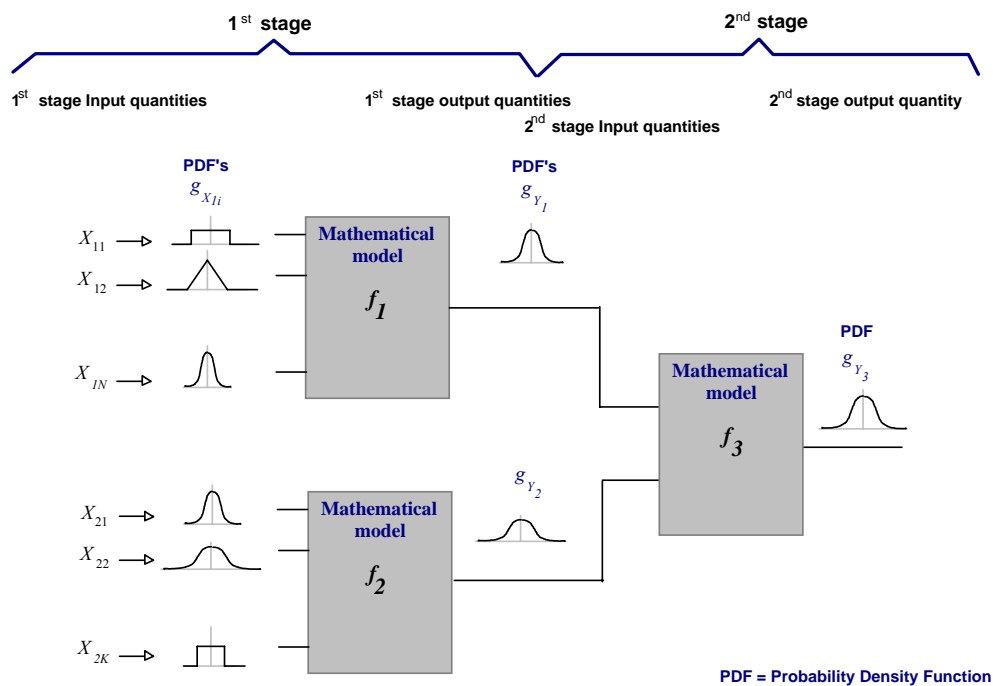


Figure 5.4: Propagation of density probability functions in a two stage measurement system

Since the MCM can be applied in the absence of mainstream GUM requirements, such as symmetry of the input probability functions (or others), the method proves to be especially suitable to be applied to non-linear mathematical models.

Development of MCM numerical simulations is carried out by generating sequences of up to 10^6 values for each quantity, depending on the required computational accuracy. The draws were based on the Mersenne Twister uniform random number generator (Matsumoto and Nishimura, 1998 – this generator is implemented in various software tools, e.g. Matlab) and the PDFs were obtained using validated methods like the Box-Muller transformation and the inverse cumulative distribution function (CDF) method (Gentle, 2004). Tests to verify the computational accuracy of the output PDFs were also made according with Cox *et al.* (2001) allowing concluding that the numerical simulations provide robust and accurate solutions for the metrological problem proposed.

In Table 5.2, the experimental input data and PDF parameters adopted are presented. Some observations to this table are:

- a. The quantity u_{max} includes the contributions from input quantities presented in Figure 5.1 (mathematical model f_1) combined with the contributions due to the resolution, linearity and drift of the indication device.
- b. The quantity $c_{us,air}$ incorporates the temperature influence of $\pm 0.17\%$ /°C and the influence of pressure of $\pm 0.1\%$ of the readings.
- c. The quantity related with the pipe diameter estimate includes the resolution effect of the measurement instrument and the roundness error effect.
- d. The quantity δh_{us} includes surface wave effects.
- e. The quantity δQ_{geom} includes effects due to pipe slopes and other geometry constrains (based on the instrumentation manufacturer information).
- f. The quantity $\delta Q_{overfalls}$ includes the geometric influence due to proximity to drops at entrance to downstream manhole.
- g. The quantity δQ_{inst_ring} includes effects due to instrumentation ring setup and installation geometry.
- h. The quantity δQ_{comp} includes effects due to computational process performed with modified off-the-shelf software.

Table 5.2: Experimental input data and PDFs adopted

| Random variables | PDF parameters | Units |
|----------------------------|----------------------------------|------------------|
| u_{max} ^{a)} | $\mathcal{N}(0.79; 0.01)$ | $m \cdot s^{-1}$ |
| C_u | $R(0.85; 0.95)$ | adim. |
| $c_{us,air}$ ^{b)} | $R(340.1; 346.9)$ | $m \cdot s^{-1}$ |
| $t_{tr,air,i}$ | $R(8.43; 8.93)$ | ms |
| D | $R(1793; 1803)$ | mm |
| d_o | $R(5; 15)$ | mm |
| δh_{us} | $R(10; 20)$ | mm |
| δQ_{geom} | $\mathcal{N}(0; 0.0025 \cdot q)$ | $L \cdot s^{-1}$ |
| $\delta Q_{overfalls}$ | $\mathcal{N}(0; 0.005 \cdot q)$ | $L \cdot s^{-1}$ |
| δQ_{inst_ring} | $\mathcal{N}(0; 0.005 \cdot q)$ | $L \cdot s^{-1}$ |
| δQ_{comp} | $\mathcal{N}(0; 0.001 \cdot q)$ | $L \cdot s^{-1}$ |

Critical conditions such as backwater flow, very low and off-axis flow velocity components and their relation with mean flow velocity were not considered given the difficulty to quantify the consequences on the measurement due to these extreme effects. However, special care should be taken when selecting the measurement locations to avoid large errors derived from this type of effects.

MCM simulations were carried out using Table 5.2 values as input parameters. The estimate of the measurement result obtained for the output quantity, volumetric flow rate, including its standard uncertainty is

$$Q_v = (229.7 \pm 14.1) L/s \quad \text{eq. 53}$$

and the related output PDF is presented in Figure 5.5.

Computation results confirm the significant advantage of using the MCM approach, since it allowed the evaluation of measurement uncertainty despite the use of a nonlinear function, f_7 ,

$$A = \frac{r_c^2}{2} \cdot \left[\arccos\left(1 - \frac{h}{r_c}\right) - \sin\left[\arccos\left(1 - \frac{h}{r_c}\right)\right] \right] \quad \text{eq. 54}$$

In fact, results are consistent, giving low computational accuracy values, as shown in Table 5.3.

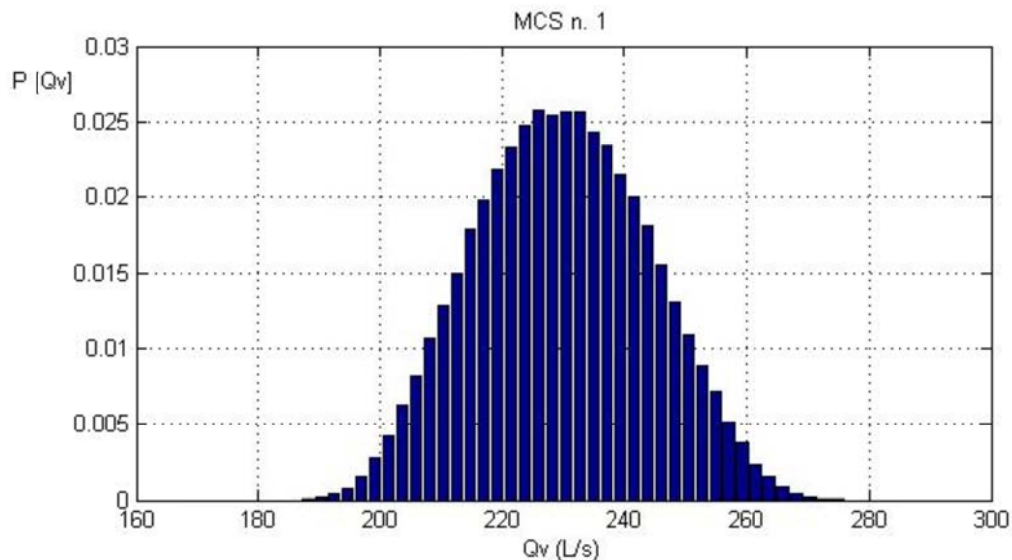


Figure 5.5: Output PDF of flow rate obtained for MCM n. 1

Table 5.3: Summary results for first set of MCM simulations

| Quantities and parameters | MCM Estimates | | |
|---------------------------|---------------|-------------|--------------|
| | MCS 1 | MCS 2 | MCS 3 |
| Volumetric flow estimate | 229.7 L/s | 229.4 L/s | 229.2 L/s |
| Standard uncertainty | 6.5 % | 902 % | 11 % |
| Computational accuracy | ± 0.15 % | ± 0.2 % | ± 0.25 % |
| Skewness | 0.04 | - 0.007 | - 0.03 |
| Excess kurtosis | - 0.50 | - 0.74 | - 0.84 |

5.4 SENSITIVITY ANALYSIS

The sensitivity analysis was developed in two ways aiming at comparing the influence of the several input quantities on the result, in order to find those that can be considered dominant and to study the effect of the geometric quantities uncertainties on the output flow measurement uncertainty.

Apparently, the output PDF has a Gaussian shape (Figure 5.5), which is the usually predicted. However, detailing the statistical study, results show a deviation from normality, namely, due to the excess kurtosis coefficient value of 0.50 (typical for a logistic distribution).

In order to study the behaviour of the output PDF and the relations with the several model parameters, a sensitivity analysis focusing the measuring uncertainties was also carried out, allowing the identification of critical parameters for the measurement uncertainty magnitude and the output PDF shape.

The sensitivity analysis clearly showed that the *wave time of transit* has the higher influence in the output measurement uncertainty. To illustrate this fact, additional MCM simulations were carried out. Overall simulations were done considering the typical standard uncertainties of $\pm 5 \cdot 10^{-5}$ s (MCS n. 01), $\pm 8 \cdot 10^{-5}$ s (MCS n. 02) and $\pm 1 \cdot 10^{-4}$ s (MCS n. 03). Results summarised in Table 5.3 show that the increase of the standard uncertainty causes an increase of both the skewness (to the right) and of the excess kurtosis coefficient, which exhibits an increasing departure from the Gaussian shape (Figure 5.6 and Figure 5.7).

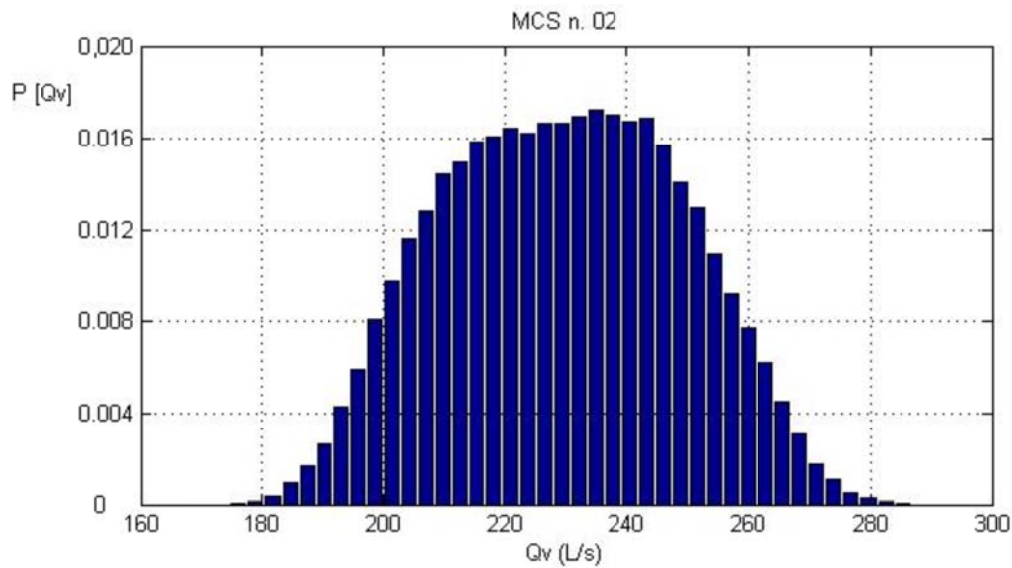


Figure 5.6: Output PDF of flow rate obtained for MCS n. 2

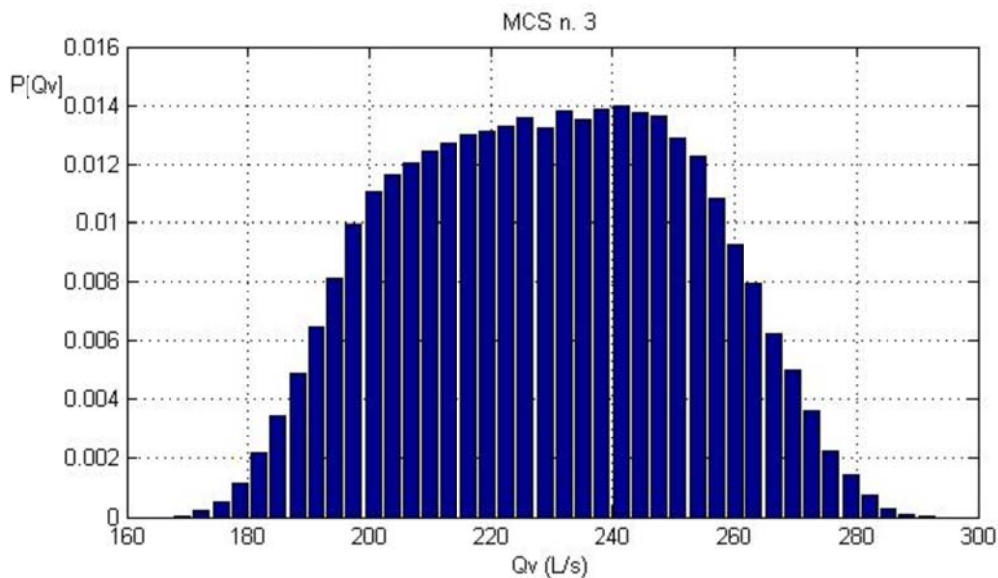


Figure 5.7: Output PDF of flow rate obtained for MCS n. 3

The PDFs presented in Figure 5.6 and Figure 5.7 support the conclusion that the output PDF is non-symmetric and non-Gaussian, and that flow rate measurement uncertainty increases significantly with the wave time transit measurement uncertainty.

The shape of the flow rate output PDF (especially the one presented in Figure 5.7) suggests the existence of an input variable with similar shape, which has large influence in certain circumstances. The analysis of the input/output quantities of the multi-stage system presented on Figure 5.1 leads to a most probable quantity, the nonlinear cross-section “wet” area, A , obtained using the function referred on eq. 54.

An MCM simulation carried out in order to obtain the output PDF associated with this variable showed that this explanation was correct. In fact, the shape of this quantity (Figure 5.8) is similar to the shape of Figure 5.6 and Figure 5.7, giving the observed non-symmetry and non-normality.

It should be emphasized that this conclusion is only possible because MCM provides the PDF information essential to this analysis. In fact, most methods to assess measurement uncertainties only provide the quantity estimates and the confidence interval limits.

Another study was carried out to assess the influence of the angle of sound propagation, β , in the output results. In fact, this influence is expected considering the direct relation between the average velocity, U , and the flow rate (see f_8).

The nominal angle is usually given as 45° , which can be difficult to establish in practice due to the mounting conditions and adverse flow conditions, as mentioned in paragraph 5.3.

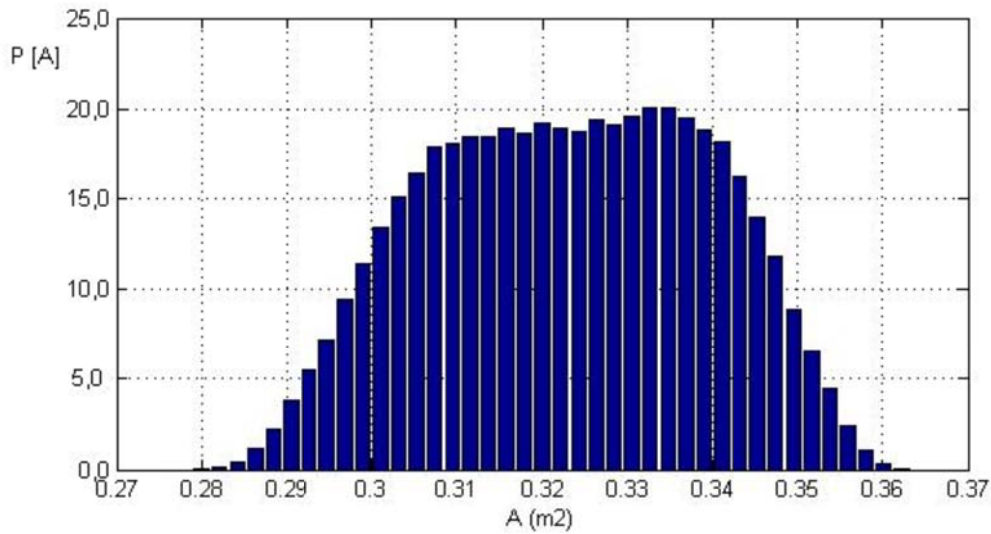


Figure 5.8: Output PDF for the cross-section "wet" area

The sensitivity analysis was performed using MCM in a two-step procedure:

- Step 1. Evaluation of the measurement uncertainty of the peak flow velocity considering a standard uncertainty of the angle β of $\pm 1\%$ (manufactures condition) or, at extreme conditions, of $\pm 5\%$;
- Step 2. Evaluation of the measurement uncertainty of the corresponding flow rate.

A synthesis of results obtained is presented in Table 5.4, showing 30 % increase in the output measurement uncertainty due to the angle uncertainty increase from $\pm 0.45^\circ$ to $\pm 2.25^\circ$ (respectively 1% and 5 % of the nominal angle of 45°). This increase is shown in Figure 5.9 and Figure 5.10 which have the same scales.

Table 5.4: Summary results for the second set of MCM simulations

| Quantity | Relative Standard uncertainty | |
|------------------------------|-------------------------------|-------------|
| | $\pm 1\%$ | $\pm 5\%$ |
| Angle (β) | $\pm 0.8\%$ | $\pm 3.9\%$ |
| Peak velocity (u_{\max}) | $\pm 6.4\%$ | $\pm 8.3\%$ |
| Flow rate (Q) | $\pm 0.8\%$ | $\pm 3.9\%$ |

Again, the use of MCM provides quantitative information regarding the relation between the input quantity (angle) and the output quantity (flow rate) based on a probabilistic approach, essential for the conclusions obtained.

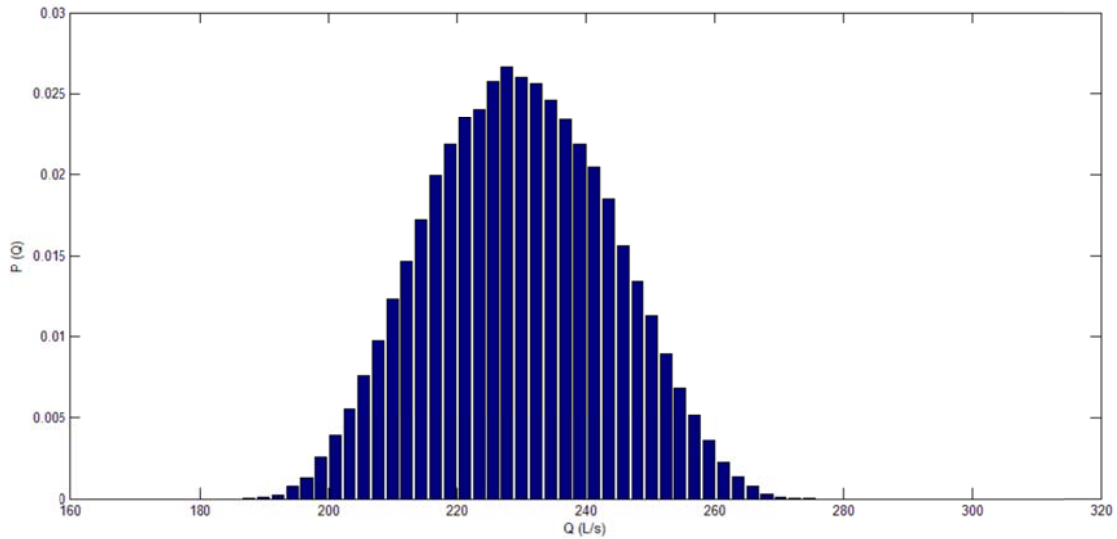


Figure 5.9: Flow rate output PDF for $u(\beta) = \pm 1 \%$

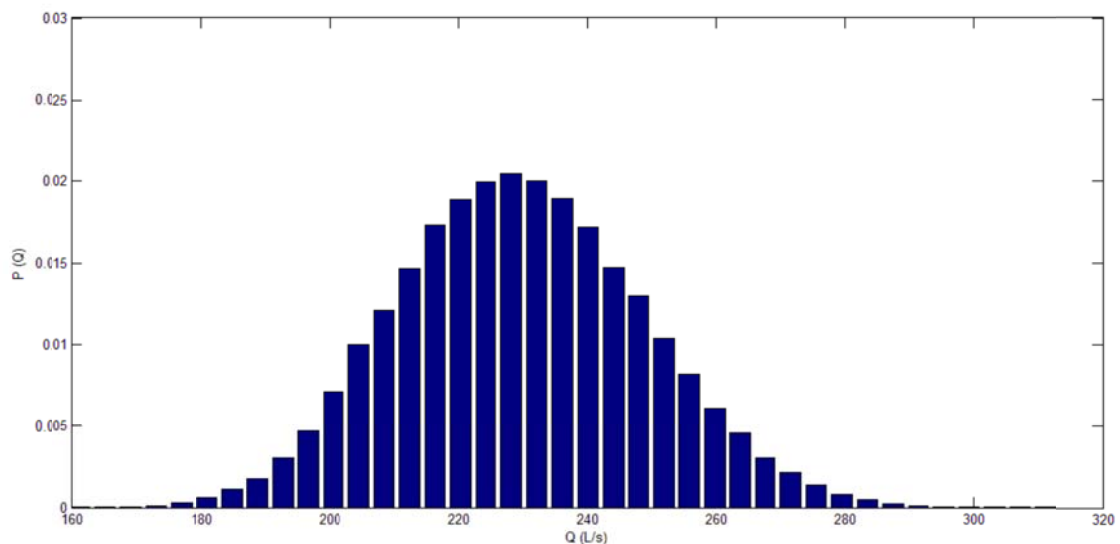


Figure 5.10: Flow rate output PDF for $u(\beta) = \pm 5 \%$

5.5 DISCUSSION AND CONCLUSIONS

The success of the evaluation of measurement uncertainties depends on the nature of the metrological problem considered, being particularly relevant the nature of the mathematical models used.

The development of metrological studies showed that the conventional GUM approach cannot lead to exact solutions when there are strongly nonlinear models, and alternative approaches such as the Monte Carlo Method have to be used, as recommended by the *Guide*.

Flow measurement in sewer systems is a typically non-linear, multi-stage metrological problem. Using the velocity area method a nonlinear relation exists on the definition of the cross-section “wet” area, therefore requiring the use of an alternative approach for determining measurement uncertainty.

In fact, the studies carried out showed that, for this type of problems, MCM is suitable to overcome the difficulties due to the nonlinear problem of the model, thus providing robust estimates of the measurement uncertainties.

Sensitivity analysis on the model parameters was carried out to define the uncertainty contributions, allowing a comparison of the sources of uncertainty effects into the output quantity (flow) uncertainty, as well as giving information on the best way to increase system accuracy. Furthermore, the analysis allowed to quantify the relation between the measurement uncertainty of the angle of sound propagation and the flow rate and to confirm the need to assure that this quantity is obtained with the best accuracy possible.

The MCM approach is also known for allowing a deeper analysis of the stochastic problems, namely, because it provides the output PDFs. This fact became especially relevant, since results showed that the output PDF can change from a nearly Gaussian shape to a non-symmetric and non-Gaussian shape depending on the individual contributions of some input quantities. This fact is significant as it increases the measurement expanded uncertainty interval.

The analysis of the data allowed concluding that the nonlinear function that provides the cross-section “wet” area generates a non-symmetric and non-Gaussian PDFs whose shape is quite similar to some of the output PDFs obtained. This conclusion can only be achieved by using a MCM approach.

This example is relevant to improve knowledge on this type of measurement systems, identifying critical points to its accuracy, to the identification of improvement opportunities, and providing useful information to support management decisions within the context of quality management.

6. REFERENCES

- AIAA. 1995. *Assessment of Wind Tunnel Data Uncertainty*. Reston, VA (USA): American Institute of Aeronautics and Astronautics, report AIAA S-071-1995.
- Bertrand-Krajewski J.-L. (2011). *Application of type B and Monte Carlo methods for UA: examples for discharge and volume measurements in a circular sewer pipe*. Villeurbanne (France): INSA Lyon, working paper prepared for the WMO – World Meteorological Organisation, 14 p. (unpublished).
- Bertrand-Krajewski J.-L., Barraud S., Lipeme Kouyi G., Torres A., Lepot M. (2007). Event and annual TSS and COD loads in combined sewer overflows estimated by continuous in situ turbidity measurements. *Proceedings of the 11th International Conference on Diffuse Pollution*, Belo Horizonte, Brazil, 26-31 August, 8 p.
- Bertrand-Krajewski J.-L., Laplace D., Joannis C., Chebbo G. (2000). *Mesures en hydrologie urbaine et assainissement [Measurements in urban drainage and sewer systems]*. Paris (France): Éditions Tec&Doc, 808 p. ISBN 2-7430-0380-4. (in French).
- Bertrand-Krajewski J.-L., Métadier M. (2010). Continuous monitoring of storm runoff quality: recent results on two experimental catchments. *Proceedings of the 2nd Regional Rainfall Conference of the Balkans*, Belgrade, Serbia, 3-5 November 2010, 12 p.
- Bertrand-Krajewski J.-L., Muste M. (2007). *Chapter 6 - Understanding and managing uncertainty*. In "Data requirements for Integrated Urban Water management", T. Fletcher and A. Deletic (editors). London (UK): Taylor and Francis, Urban Water series - UNESCO IHP, 65-90. ISBN 9780415453455.
- Cox M.G., Dainton M.P., Harris P.M. (2001). *Software specifications for uncertainty calculation and associated statistical analysis*. Teddington (UK): National Physical Laboratory, NPL Report CMSC 10/01, 46 p.
- Edelhauser M. (1999). *A Comparison of Continuous Wave Doppler vs. Pulsed Doppler Profiling Technology*. San Diego, CA (USA) : MGD Technologies Inc., February 1999.
- ENV 13005 (1999). *Guide pour l'Expression de l'Incertitude de Mesure [Guide to the Expression of Uncertainty in Measurement]*. Paris (France): AFNOR (Association Française de Normalisation), August 1999, 113 pp.
- Fletcher T.D., Deletic A. (2007). Statistical Observations of a Stormwater Monitoring Programme; Lessons for the Estimation of Pollutant Loads). *Proceedings of Novatech 2007*, Lyon, France, 25-28th June, 8 p.
- Gentle J. E. (2004). *Random Number Generation and Monte Carlo Methods*. New York (USA): Springer-Verlag, 2nd edition, 264 p. ISBN 978-0387001784.
- Gruber G., Winkler S., Pressl A. (2005). Continuous monitoring in sewer networks: an approach for quantification of pollution loads from CSOs into surface water bodies. *Water Science and Technology*, 52(12), 215-223.
- GUM (1993). *Guide to the Expression of Uncertainty in Measurement*. Geneva (Switzerland): ISO.
- ISO (2005). *ISO 5168. Measurement of Fluid Flow – Procedures for the Evaluation of Uncertainties*. Geneva(Switzerland): ISO, August 2005, 65 p.
- ISO (2008a). *ISO/IEC Guide 98-3:2008(E) Uncertainty of measurement - Part 3: Guide to the expression of uncertainty in measurement (GUM:1995)*. Geneva (Switzerland): ISO, December 2008, 130 p.
- ISO (2008b). *ISO/IEC Guide 98-3/Suppl.1:2008(E) Uncertainty of measurement - Part 3: Guide to the expression of uncertainty in measurement (GUM:1995) Supplement 1: Propagation of distributions using a Monte Carlo method*. Geneva (Switzerland): ISO, December 2008, 98 p.
- ISO (2009a). *ISO/IEC Guide 98-1:2009(E) Uncertainty of measurement – Part 1: Introduction to the expression of the uncertainty in measurement*. Geneva (Switzerland): ISO, September 2009, 32 p.
- ISO (2009b). *ISO/IEC Guide 98-3/S1/AC1:2009(E) Uncertainty of measurement - Part 3: Guide to the expression of uncertainty in measurement (GUM:1995), Supplement 1: Propagation of distributions using a Monte Carlo method, Technical corrigendum 1*. Geneva (Switzerland): ISO, May 2009, 2 p.
- Jaafar W., Fischer S., Bakkour K. (2009). Velocity and turbulence measurements by ultrasound pulse Doppler velocimetry. *Measurement*, 42(2), 175-182.
- JCGM (2008). *JCGM 200:2008 – International Vocabulary of metrology – Basic and general concepts and associated terms (VIM) – 3rd edition*. Sèvres (France): BIPM – Bureau International des Poids et Mesures, 104 p. Freely available at http://www.bipm.org/utis/common/documents/jcgm/JCGM_200_2008.pdf
- JCGM (2010). *JCGM 200:2008 – International Vocabulary of metrology – Basic and general concepts and associated terms (VIM) – 3rd edition - Corrigendum*. Sèvres (France): BIPM – Bureau International des Poids et Mesures, May 2010, 23 p.
Available at http://www.bipm.org/utis/common/documents/jcgm/%20JCGM_200_2008_Corrigendum.pdf
- Joannis C., Bertrand-Krajewski J.-L. (2009). Incertitudes sur un mesurande défini comme une valeur intégrée d'un signal continu discrétisé en fonction du temps - Application aux mesures hydrologiques enregistrées in

- situ [Uncertainty in a measurand defined as the integrated value of a continuous signal discretised in time]. *La Houille Blanche*, 3, 82-91. (in French).
- Lacour C. (2009). *Apport de la mesure en continu pour la gestion de la qualité des effluents de temps de pluie en réseau d'assainissement [Interest of continuous monitoring for the control of water quality during wet weather in sewer systems]*. PhD thesis: Université Paris Est, Marne la Vallée, France, 278 p. (in French).
- Larrarte F. (2006). Velocity fields within sewers: An experimental study. *Flow Measurement and Instrumentation*, 17, 282-290.
- Lepot M., Bertrand-Krajewski J.-L., Lipeme-Kouyi G. (2010). Vérification des mesures de débit en réseau d'assainissement par traçage à la Rhodamine [Verification of discharge measurements in sewer systems by Rhodamine tracing experiments]. *Actes des 4^e Journées Doctorales en Hydrologie Urbaine "JDHU 2010"*, Marne-la-Vallée, France, 16-17 novembre 2010, 48-55. (in French).
- Matsumoto M., Nishimura T. (1998). Mersenne Twister: a 623-dimensionally equidistributed uniform pseudorandom number generator. *ACM Transactions on Modelling and Computer Simulations*, 8(1), 3-30.
- Métadier M., Bertrand-Krajewski J.-L. (2011). From mess to mass: a methodology for calculating storm event pollution loads with their uncertainties, from continuous raw data. *Water Science and Technology*, 63(3), 369-376.
- Métadier M., Bertrand-Krajewski J.-L. (2010b). Assessing dry weather flow contribution in TSS and COD storm events loads in combined sewer systems. *Proceedings of Novatech 2010*, Lyon, France, 27 June - 1 July, 10 p.
- Moffat R.J. (1988). Describing the Uncertainties in Experimental Results. *Experimental Thermal and Fluid Science*, 1(1), 3-17.
- Muste M., Lee K., Bertrand-Krajewski J.-L. (2011). Standardized Uncertainty Analysis for Hydrometry: Review of Relevant Approaches and Implementation Examples. *Hydrological Sciences Journal* (submitted).
- Schilperoort R.P.S., Dirksen J., Langeveld J.G., Clemens F.H.L.R. (2009). Assessing characteristic time and space scales of in-sewer processes by analysis of one year of continuous in sewer monitoring data. *Proceedings of the 8th UDM - International Conference on Urban Drainage Modelling*, Tokyo, Japan, 7-12 September, 8 p.
- Ribeiro A.S., Almeida M.C., Palma J. (2009). Uncertainty evaluation of multi-sensor flow measurement in a sewer system using Monte Carlo method. *Proceedings of the XIX IMEKO World Congress on Fundamental and Applied Metrology*, Lisbon, Portugal, 6-11 September, 6 p.
- Torres A. (2008). *Décantation des eaux pluviales dans un ouvrage réel de grande taille: éléments de réflexion pour le suivi et la modélisation [Settling of stormwater in a large storage tank: contribution to monitoring and modelling]*. PhD thesis: INSA de Lyon, France, 374 p. (in French). <http://docinsa.insa-lyon.fr/these/pont.php?id=torres>